*Mineralogical Magazine, February 2018, Vol. 82(1), pp. 35–58*

# Mineralogy of the Vattikod lamproite dykes, Ramadugu lamproite field, Nalgonda District, Telangana: A possible expression of ancient subduction-related alkaline magmatism along Eastern Ghats Mobile Belt, India

Gurmeet Kaur*[,1,2], Roger H. Mitchell[2] and Suhel Ahmed[3]

[1] Department of Geology, Panjab University, Chandigarh UT-160014, India
[2] Department of Geology, Lakehead University, Thunder Bay, Ontario P7B 5E1, Canada
[3] Geological Survey of India, Southern Region, Hyderabad - 500 068, Andhra Pradesh, India

[*Received 5 December 2016; Accepted 4 June 2017; Associate Editor: Brian O'Driscoll*]

**ABSTRACT**

The mineralogy of nine recently discovered dykes (VL1:VL8 and VL10) in the vicinity of Vattikod village, Nalgonda district in Telangana State is described. The mineral assemblage present and their compositions are comparable to those of bona fide lamproites in terms of the presence of phlogopite (Ti-rich, Al-poor phlogopite and tetraferriphlogopite); amphiboles (potassic-arfvedsonite, potassic-richterite, potassic-ferro-richterite, potassic-katophorite, Ti-rich potassic-katophorite, Ti-rich potassic-magnesio-katophorite); Al-poor clinopyroxenes; feldspars (K-feldspar, Ba-K-feldspar and Na-feldspar) and spinels (chromite-magnetite and qandilite-ulvöspinel-franklinite). These dykes have undergone diverse and significant degrees of deuteric alteration as shown by the formation of secondary phases such as: titanite, allanite, hydro-zircon, calcite, chlorite, quartz and cryptocrystalline $SiO_2$. On the basis of their respective mineralogy: the VL4 and VL5 dykes are classified as pseudoleucite-phlogopite lamproite; VL2 and VL3 dykes as pseudoleucite-amphibole-lamproite; and VL6, VL7 and VL8 as pseudoleucite-phlogopite-amphibole-lamproite. VL10 is extensively altered but contains fresh euhedral apatite microphenocrysts together with pseudomorphs after leucite and is classified as a pseudoleucite-apatite-(phlogopite?) lamproite. The mineralogy of the Vattikod lamproite dykes is compared with that of the Ramadugu, Somavarigudem and Yacharam lamproite dykes which also occur in the Ramadugu lamproite field. The lamproites from the Eastern Dharwar Craton are considered as being possible expressions of ancient subduction-related alkaline magmatism along the Eastern Ghats mobile belt.

**Keywords:** lamproite, pseudoleucite, phlogopite, K-Na-amphiboles, Vattikod, Eastern Dharwar Craton, subduction.

## Introduction

Lamproites are mantle-derived, volatile-rich alkaline igneous rocks. These rocks are unusual in terms of their mineralogy and economically very important with respect to their diamond potential (Mitchell and Bergman, 1991; Mitchell, 1995). Lamproite magmas have been considered as originating in two broad tectonic environments: (1) subduction settings and commonly termed Mediterranean lamproites (Mitchell and Bergman, 1991; Conticelli, 1998; Murphy *et al*., 2002; Prelević *et al.* 2008; Tommasini *et al*., 2011; Fritschle *et al.,* 2013; Perez-Valera *et al.,* 2013) or (2) within-plate cratonic regions (Leucite Hills, West Kimberley; Mitchell and Bergman, 1991; Mitchell, 1995). Lamproite magmas might originate from sources varying from the sub-continental

*E-mail:gurmeet28374@yahoo.co.in
https://doi.org/10.1180/minmag.2017.081.045

lithospheric mantle to asthenospheric and deeper mantle material (Tainton and McKenzie, 1994; Mitchell, 1995; Murphy *et al*., 2002; Nowell *et al*., 2004; Davies *et al.*, 2006; Mirnejad and Bell, 2006; Chakrabarti *et al*., 2007; Rapp *et al.*, 2008; Mitchell and Tappe, 2010; Tappe *et al*., 2007, 2013).

The identification of a suite of rocks as lamproite or kimberlite relies on detailed mineralogical studies to establish the presence or absence of typomorphic minerals (Mitchell and Bergman, 1991, Mitchell, 1995). Identification of lamproites on the basis of their bulk-rock geochemistry is possible only for fresh rocks. Note that unless the rocks are glassy the whole-rock composition is actually determined by the mineralogy and not *vice versa*. The analysis of altered rocks is not a useful endeavour and can lead to completely inappropriate genetic conclusions. In this work, using a mineralogical-genetic system (Mitchell, 1995; Mitchell and Bergman, 1991) we classify the dyke rocks in the Vattikod area as *bona fide* lamproites and show these to be members of a suite of lamproites emplaced along the eastern margins of the Eastern Dharwar Craton (Ahmed and Kumar, 2012; Kumar *et al*., 2013*a*; Chalapathi Rao *et al*., 2014). On the basis of our classification we make further inferences as to the role of subduction in their genesis but no claims that these rocks are analogous to young Mediterranean-type lamproites. Rather, they are considered as rocks crystallized from magmas originating from ancient metasomatized lithospheric mantle which contains a subducted component (Chalapathi Rao *et al*., 2004; Mitchell, 2006; Chakrabarti *et al*., 2007; Das Sharma and Ramesh, 2013; Gurmeet Kaur and Mitchell, 2013; Gurmeet Kaur and Mitchell, 2016; Gurmeet Kaur *et al.,* 2016).

## Dharwar Craton lamproites

The Dharwar Craton contains numerous kimberlites and lamproites (Neelkantam, 2001; Fareeduddin and Mitchell, 2012; Chalapathi Rao and Srivastava, 2016; Shaikh *et al*., 2016). These rocks are disposed almost parallel to the interface of the juxtaposed Eastern Ghats Mobile Belt and the Eastern Dharwar Craton (Fig. 1; Neelkantam, 2001; Fareeduddin and Mitchell, 2012; Gurmeet Kaur and Mitchell, 2016). The lamproite fields in the Eastern Dharwar Craton are: (1) The P2-West, P12, P5, P13, TK1 and TK4 intrusions of Wajrakarur field; (2) the Chelima, Zangamarajupalle, Garledinne, Banganapalle lamproites of the Cuddapah Basin; (3) the Krishna lamproite field; and (4) the Ramadugu lamproite field (Fareeduddin and Mitchell, 2012; Gurmeet Kaur *et al.*, 2013; Gurmeet Kaur and Mitchell, 2013; Gurmeet Kaur and Mitchell, 2016; Chalapathi Rao and Srivastava, 2016 and references therein; Shaikh *et al.,* 2016). Many of the above rocks were considered previously to be 'kimberlites' in previous investigations but are now reclassified as lamproites (see Fareedudddin and Mitchell, 2012 and references therein; Gurmeet Kaur *et al.*, 2013; Gurmeet Kaur and Mitchell, 2013; Gurmeet Kaur and Mitchell, 2016; Shaikh *et al*., 2016).

New hypotheses on the nature of the crust-mantle lithosphere components of Eastern Dharwar Craton have been proposed on the basis of seismic tomographical studies. The crustal thickness of 33–39 km with a Moho depth of ~40 km and an average heat flow of $36 \pm 8$ mW/m$^2$ has been evaluated for the Eastern Dharwar Craton (Gupta *et al.*, 2003; Roy and Mareschal, 2011; Kumar *et al*., 2013*b*). Of particular importance with respect to lamproite genesis, Das Sharma and Ramesh (2013) suggest that a thick lithospheric root underlies southeast India, with the Archaean Eastern Dharwar Craton and the Proterozoic Eastern Ghats Mobile Belt being underlain by a relict subducted slab within the upper mantle.

## Ramadugu lamproite field

The Ramadugu lamproite field was discovered by Sridhar and Rau (2005) in the Nalgonda district of Telangana state (formerly Andhra Pradesh) during a diamond exploration programme initiated by the Geological Survey of India along the Krishna River. The Ramadugu lamproite field lies northwest of the Cuddapah Basin and close to the Krishna lamproites in the east (Fig. 1). The Ramadugu lamproite field consists of dykes occurring at Ramadugu, Somavarigudem, Yacharam and Vattikod (Fig. 2). The Ramadugu lamproites are emplaced in granodiorites and granites of the Peninsular Gneissic Complex of the Eastern Dharwar Craton (Fig. 2). The lamproite dykes have a general NW-SE strike with variable lengths from a few metres to ~700 m, with a maximum width of 3.5 m (Sridhar and Rau, 2005; Ahmed and Kumar, 2012; Kumar *et al*., 2013*a*; Chalapathi Rao *et al*., 2014). The lamproites occurring in the Krishna, Nallamalai and Ramadugu lamproite fields are diamondiferous (Chalapathi Rao *et al*., 2014).



https://doi.org/10.1180/minmag.2017.081.045 Published online by Cambridge University Press

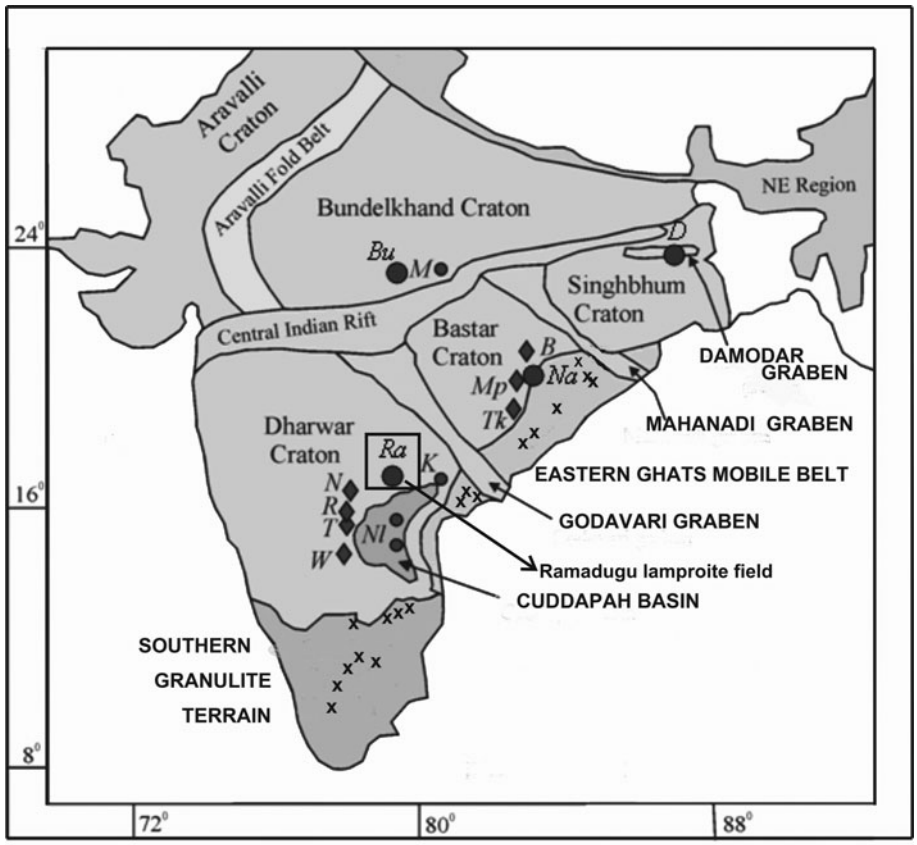


FIG. 1. Distribution of kimberlites and lamproites in the Bundelkhand, Singhbhum, Bastar and Dharwar cratons of the Indian subcontinent. Diamonds (♦), circles (●) and crosses (x) in the figure refer to kimberlites, lamproites and deformed alkaline rocks and carbonatites (DARC) locations in the southern Indian sub-continent, respectively. Bu – Bunder lamproites, M – Majhgawan lamproite field, B – Basna kimberlite field, Na – Nawapara lamproite field, Mp – Mainpur kimberlite field, Tk – Tokapal kimberlite field, Ra – Ramadugu lamproite field, N – Narayanpet kimberlite field, R – Raichur kimberlite field, T – Tungabhadra kimberlite field, W – Wajrakarur kimberlite field, Nl – Nallamalai lamproite field, K – Krishna lamproite field, and D – Damodar valley lamproites (Gurmeet Kaur and Mitchell, 2016).

## Vattikod dykes

The Vattikod lamproite dykes, within the Ramadugu lamproite field, were discovered by Ahmed and Kumar (2012). The ten dykes (VL1: VL10) are spread over an area of ~6 square km to the west of Vattikod village (N16°55'13.2″ E79° 05'55″) and ~22 km north-west of Ramadugu village (Fig. 2; modified after Kumar *et al.*, 2013*a*). The dyke swarm follows a WNW-ESE to NW-SE trend traversing the Peninsular Gneissic Complex (Fig. 2). The lengths of the dykes are difficult to ascertain as most are covered by soil (Supplementary Figure S1, see below).

Nine dyke samples, VL1 to VL8 and VL10, were collected during March 2014 from the vicinity of Vattikod village. Brief field records of the occurrence are given in Table 1. (For detailed field records refer to the report of Ahmed and Kumar (2012) and Kumar *et al.* (2013*a*).

A very brief general account of the petrology of a few Vattikod dykes was given by Kumar *et al.* (2013*a*). In the present study each dyke was characterized on the basis of its major, minor and accessory mineralogy. We also attempt to determine the sequence of evolution of these nine dykes on the basis of their typomorphical mineralogy. The mineralogy of the Vattikod dykes is compared



https://doi.org/10.1180/minmag.2017.081.045 Published online by Cambridge University Press

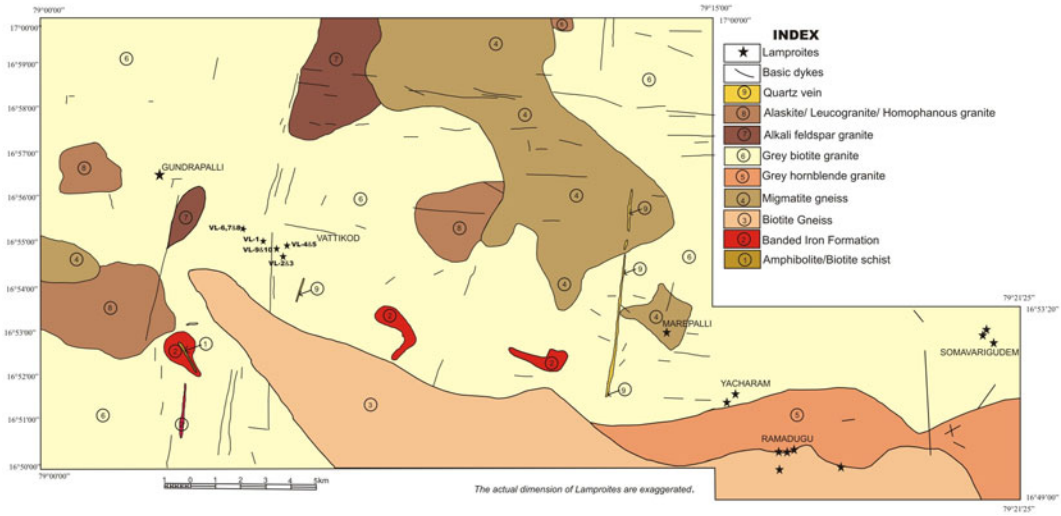


FIG. 2. Ramadugu lamproite field consisting of the Ramadugu, Yacharam, Somavarigudem and Vattikod lamproite dykes, Nalgonda district, Telangana, India. The location of Vattikod lamproites and other Ramadugu lamproite dykes are marked on the map.

with that of the Ramadugu, Somavarigudem and Yacharam lamproite dykes, which also form part of the Ramadugu lamproite field and lie to the southeast of the Vattikod dykes.

## Analytical techniques

Representative samples of Vattikod lamproites were investigated by back-scattered electron (BSE) imagery and quantitative energy-dispersive X-ray spectrometry using a Hitachi SU-70 scanning electron microscope at Lakehead University, Ontario, Canada. All raw X-ray data were acquired using a beam current of 300 pA, an accelerating voltage of 20 kV and 30–60 s counting times and processed using Oxford *Aztec* software. Standards used are those given by Liferovich and Mitchell (2005).

## Petrography and mineralogy of Vattikod dykes

The Vattikod dykes are fine-grained rocks with phenocrysts and microphenocrysts of pseudoleucite, phlogopite, clinopyroxene, apatite and pseudomorphed olivine (Figs 3–7). Phlogopite and apatite are the only preserved phenocryst and microphenocryst primary phases (Figs 4*c*, 6*c*), as all other phenocryst phases such as leucite, clinopyroxene and olivine have been pseudomorphed by K-feldspar, calcite, apatite, chlorite,

TABLE 1. Details of Vattikod lamproite dykes, Ramadugu lamproite field, Telangana, India (modified after Kumar *et al.*, 2013*b*).

| Dyke Nos. | Dimensions | Trends | Latitude and Longitude details |
|---|---|---|---|
| VL1 | 1.7 m wide | N72°W | N16°55’07.5”, E79°05’05.2” |
| VL2, VL3 | 639 m long, 2 m wide | N60°W | N16°54’59.3”; E79°05’18.4” |
| VL4 | 4.3 m long, 0.15 m wide | N60°W | N16°55’02.1”; E79°05’19.5” |
| VL5 | 7 m long, 0.15–0.30 m wide | N47°W – N70°W | |
| VL6 | 50 m long, 0.65 m wide | N50°W – N60°W | N16°55’21.6”; E79°04’21.7” |
| VL7 | 20 m long, 0.28 m wide | | |
| VL8 | 3 m long, 0.08–0.10 m wide | | |
| VL10 | 8.4 m long, 0.60 m wide | N80°E | N16°54’58.7”; E79°05’28.3” |



https://doi.org/10.1180/minmag.2017.081.045 Published online by Cambridge University Press

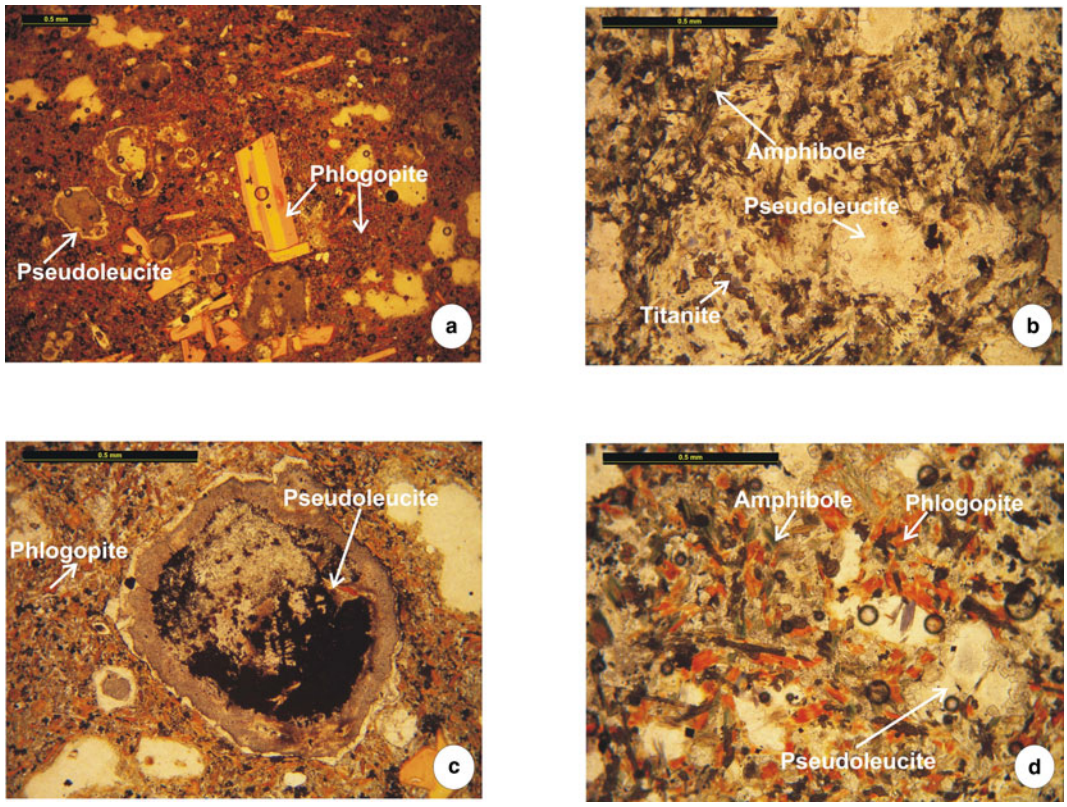


FIG. 3. Plane-polarized light images: (*a*) the texture of the VL2 showing greenish-brown prismatic amphiboles, ovoid pseudoleucites, and groundmass titanite aggregates in fine grained matrix; (*b*) the texture of the VL5 lamproite dyke illustrating the presence of phenocrysts of phlogopite-tetraferriphlogopite and pseudoleucite set in a fine-grained groundmass material with predominant phlogopite; (*c*) flow texture around pseudoleucite in VL 5; and (*d*) the texture of VL6 with amphiboles, phlogopites and pseudoleucites set in a fine-grained groundmass.

quartz and cryptocrystalline $SiO_2$ (Figs 3*b*,*c*, 4*a*, 6*b*). The phenocryst and microphenocryst phases are set in a fine-grained matrix composed of phlogopite–tetraferriphlogopite, amphibole, clinopyroxene, K-feldspar (pseudoleucite), spinel, apatite, monazite, calcite, baryte, titanite, rutile and allanite. The mesostasis in which the above minerals are set is composed of chlorite, quartz and cryptocrystalline $SiO_2$. Other minor phases are dolomite, magnetite, pyrite, Ba-K-feldspar, Na-feldspar, hydro-zircon, strontianite and Co-Ni-bearing copper sulfides. Clasts composed of finer-grained material have been observed in VL2 and VL4. These clasts consist of material very similar to the groundmass phases in VL2 and VL4. The VL2 clasts contain more titanite, rutile, hydro-zircon, cryptocrystalline $SiO_2$ and magnetite in comparison to VL2 groundmass which has more pseudoleucite, amphibole, apatite and chlorite (Fig. 4*b*). The VL4 clasts have more rutile and cryptocrystalline $SiO_2$ and less calcite and K-feldspar, in comparison to a groundmass of VL4.

Phlogopite occurs as phenocrysts, microphenocrysts and as a groundmass phase. Phlogopite phenocrysts and microphenocrysts are prominent in dyke VL5 and are rarely preserved in the other dykes due to diverse degrees of alteration. Phlogopites are zoned, and exhibit the typical yellow-orange pleochroism of lamproite phlogopite together with thin rims of dark red tetraferriphlogopite (Fig. 3*a*). Phlogopites in VL5 are devoid of inclusions, and unaltered (Fig. 4*c*) in comparison to phlogopites in other dykes which have corroded margins, are poikilitic, and show alteration to chlorite (Fig. 4*d*). The poikilitic phlogopites commonly have inclusions of apatite, spinel,



https://doi.org/10.1180/minmag.2017.081.045 Published online by Cambridge University Press

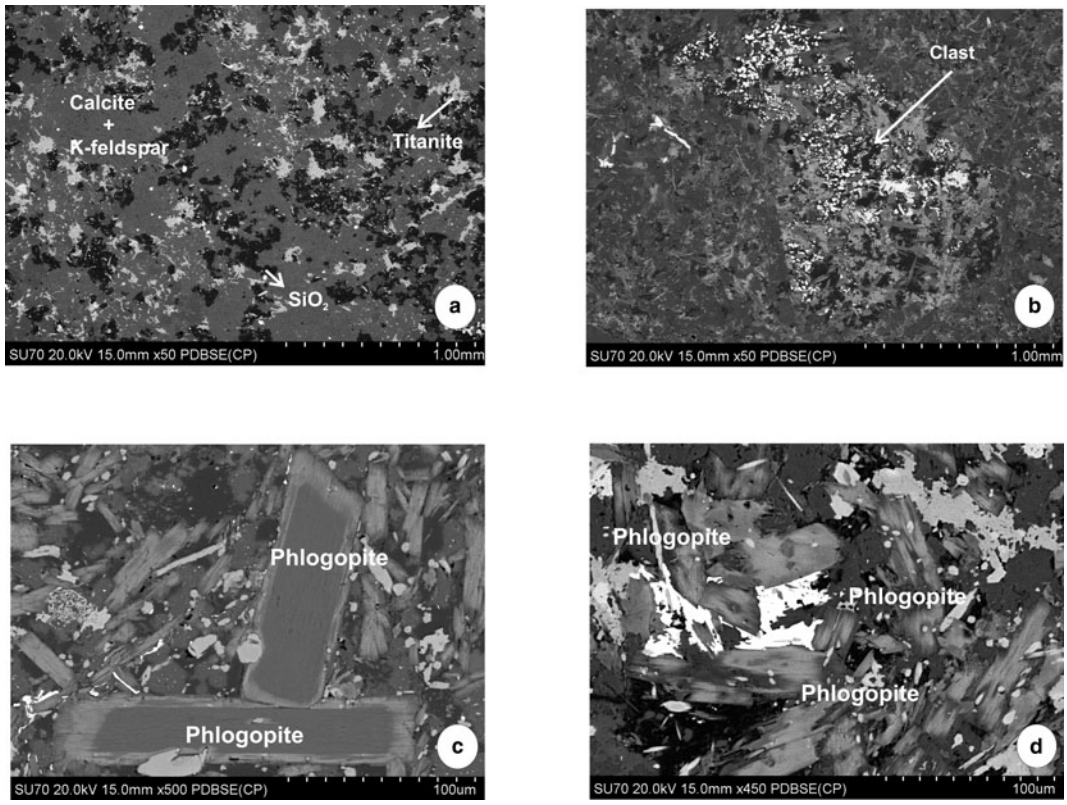


FIG. 4. BSE images: (*a*) calcite- K-feldspar pseudomorph, titanite and cryptocrystalline $SiO_2$ in highly altered VL1 dyke; (*b*) finer grained clast enriched in rutile, hydro-zircon, titanite and cryptocrystalline $SiO_2$ in VL2 dyke; (*c*) zoned microphenocryst of phlogopites set in groundmass material enriched in phlogopites in VL5; and (*d*) groundmass phlogopites altering to chlorite in VL8.

clinopyroxene and chlorite. Most of the phenocrysts and microphenocrysts of phlogopites in other Vattikod dykes are pseudomorphed by chlorite, titanite and allanite (Fig. 6*a*). Titanite and allanite occur mainly along the cleavage planes and margins of the altered phlogopites. Groundmass phlogopite occurs in VL4, VL5, VL6, VL7, VL8 and is negligible-to-subordinate in VL2 and VL3 dykes. In VL1 phlogopite has not been identified, whereas the former presence of phlogopites in VL10 is suggested by the presence of chlorite pseudomorphs. Dykes VL4 and VL5 preserve the freshest groundmass phlogopites. The phlogopites in VL6, VL7 and VL8 are partially- to- almost completely- altered to chlorite whereas phlogopites in VL2 and VL3 are almost completely altered to chlorite. Groundmass micas are tetraferriphlogopites, which are identified by their reddish reverse pleochroism (Figs 3*d*). The VL5 groundmass phlogopites exhibit a flow texture (Figs. 3*c*, 6*b*), which is unique relative to phlogopites in all other Vattikod dykes.

Amphiboles are a common groundmass phase in the VL2, VL3, VL6, VL7 and VL8 dykes and occur as zonation-free slender prisms and as wedge-shaped, euhedral crystals (Figs 5*a–d*). The crystals range in size from 200–10 μm. The amphiboles are both zoned and zonation-free. The zoned amphibole can have three different zones (Fig. 5*d*; Table 3). The amphiboles are associated with apatite, hydro-zircon (Fig. 5*a*), allanite (Fig. 5*b*) and baryte (Fig. 5*c*), and can be enclosed within rutile grains (Fig. 5*d*). Clinopyroxene occurs as microphenocrysts and as a groundmass phase (300–30 μm) in dykes VL2, VL3 and VL7 and are subordinate in comparison to amphiboles. Most of the clinopyroxenes are altered to chlorite (Figs 6*a*). In places, pseudomorphs of magnesian chlorite



https://doi.org/10.1180/minmag.2017.081.045 Published online by Cambridge University Press

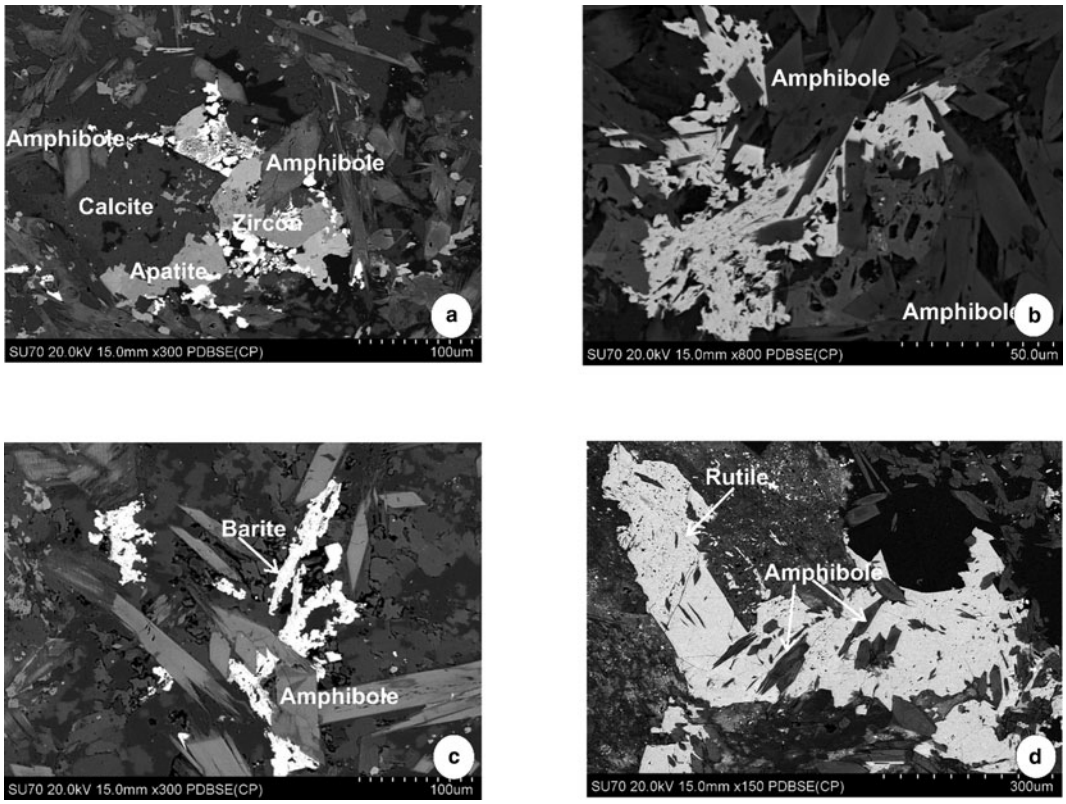


FIG. 5. BSE images: (*a*) euhedral prismatic and wedge shaped amphiboles, both zoned and unzoned in VL2 in association with groundmass calcite, hydro-zircon, and apatite; (*b*) euhedral-to-subhedral amphiboles in association with allanite in VL6; (*c*) euhedral-to-subhedral amphiboles in association with baryte in VL6; and (*d*) amphiboles completely enclosed inside rutile in VL8.

after clinopyroxene have developed titanite and calcite rims.

The most common mineral in the Vattikod dykes is K-feldspar which occurs as phenocrysts and microphenocrysts, pseudomorphs after leucite, and as fine-grained groundmass material. That the pseudoleucite represents former primary leucite is a conclusion drawn from the typical habit of the pseudomorphs (Figs 3*b*,*c*). In dykes VL6, VL7 and VL8, most of the leucite pseudomorphs contain hydro-zircon aggregates occupying the core together with K-feldspar and calcite (Fig. 6*b*). K-feldspar, calcite, apatite, chlorite, Na-feldspar and K-Ba feldspar (hyalophane) are also components of the pseudomorphs. The groundmass K-feldspars also form small ovoids (<50 μm) mostly formed after leucites (Fig. 3*b*,*d*). K-feldspar is also found as an interstitial material which is considered to be a late-stage crystallization phase. Fresh leucite has not been observed in any of the Vattikod dykes.

Spinel occurs as euhedral-to-subhedral crystals (<50 μm) as a groundmass phase (Fig. 7*a*). It also occurs within, or at, the margins of some of the phenocrystal phases such as pseudoleucites and pseudomorphed phlogopites. The groundmass spinels are both zoned and zonation-free. Apatite occurs as a phenocryst- to- microphenocryst phase in dykes VL2, VL3 and VL10 (Fig. 6*c*). Groundmass apatite occurs principally as euhedral-to-subhedral grains (50–5 μm), and as anhedral aggregates (Fig. 6*d*). Apatite crystals are also poikilitically-enclosed by groundmass phlogopites together with titanite aggregates. Apatites are also associated closely with other groundmass phases such as titanite, rutile, calcite, monazite and hydro-zircon (Fig. 6*d*). Monazite-(Ce) occurs as a late-



https://doi.org/10.1180/minmag.2017.081.045 Published online by Cambridge University Press

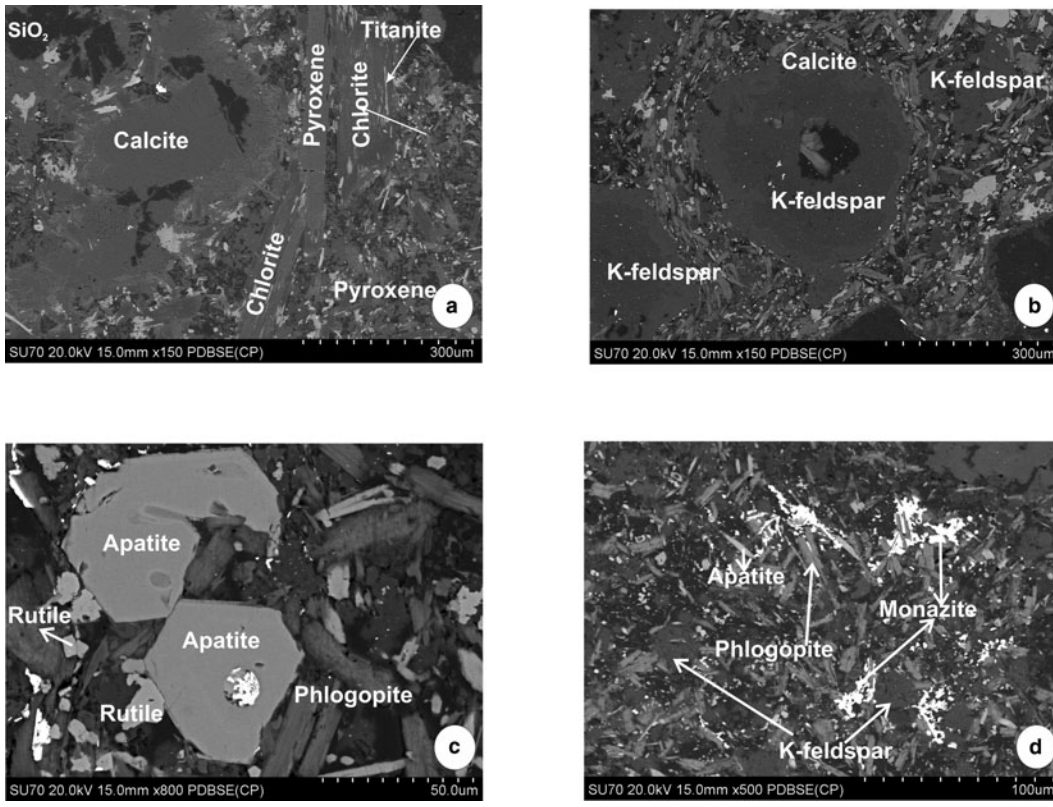


FIG. 6. BSE images: (*a*) development of titanite along the cleavage planes of a prismatic ferromagnesian mineral (phlogopite/pyroxene?) now pseudomorphed by chlorite; (*b*) K-feldspar and calcite pseudomorph after leucite in VL5, with a clear flow texture in VL5 visible; (*c*) euhedral groundmass apatites in VL5, with rutile grains visible; and (*d*) anhedral patches of monazite in VL4 along with groundmass phlogopites.

stage anhedral groundmass phase (up to 50 μm) in VL4 and VL5 dykes (Fig. 6*d*). Monazite occurs in association with phlogopite, apatite, K-feldspar, calcite and cryptocrystalline $SiO_2$.

Titanite, allanite, calcite, baryte and hydro-zircon are ubiquitous groundmass phases in all of the Vattikod dykes (Figs 7*a–d*). Titanite occurs primarily as: (1) aggregates forming part of the groundmass; (2) inside, and along, the margins of the pseudomorphs after leucite, clinopyroxene and phlogopite. The titanite of parageneses (1) seems to be a late-stage phase in the groundmass, whereas paragenetic type (2) is secondary phase formed as a result of alteration/reaction between some phases and deuteric fluids. Rutile in the dykes occurs as a late-stage mineral in variable sizes as subhedral-to-euhedral crystals (100 μm to <5 μm), and is associated commonly with titanite, apatite and hydro-zircon. Allanite occurs as aggregates forming part of the groundmass and is commonly seen replacing chlorite pseudomorphs (Figs 7*c*,*d*). Rutile is not a common phase in lamproites but has been reported from Raniganj lamproites (Mitchell and Fareeduddin, 2009). Rutile is reported from Somavarigudem lamproite dykes of Ramadugu lamproite field (Chalapathi Rao *et al*., 2014). Rutile is a common phase in ultramafic lamprophyres and calcite kimberlites (Zurevinski and Mitchell, 2011; Tappe *et al*., 2006, 2014). Allanites have not been previously recognized in Vattikod and other Ramadugu lamproites (Kumar *et al*., 2013*a*; Chalapathi Rao *et al*., 2014). Titanites are not primary phases and have formed as a result of deuteric alteration. Titanites, both primary and secondary, have been reported from other Ramadugu lamproites by Chalapathi Rao *et al*., (2014).



https://doi.org/10.1180/minmag.2017.081.045 Published online by Cambridge University Press

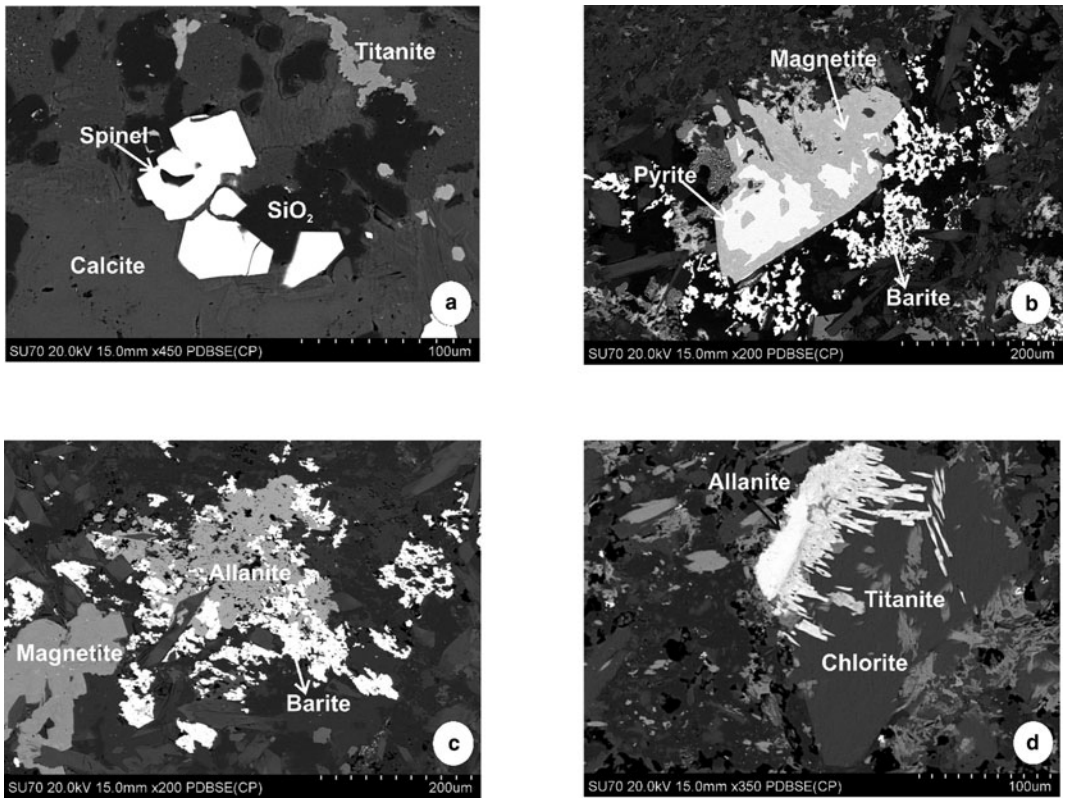


FIG. 7. BSE images: (*a*) subhedral spinels inside leucite pseudomorphs; (*b*) intergrown magnetite and pyrite in VL6; (*c*) aggregate of allanite and baryte in the groundmass of VL6; and (*d*) allanite and titanite replacing an earlier phase along the margins, which is now chlorite in VL10.

Calcite occurs as a groundmass phase forming: (1) late-stage aggregates (Fig. 5*a*); and (2) pseudomorphs after some earlier-crystallized minerals such as leucite, pyroxene (Fig. 6*b*). The groundmass calcites in almost all dykes are probably late-stage residual phases as they fill the interstitial spaces between the earlier-formed groundmass phases (Fig. 5*a*). Baryte occurs as anhedral patches in the groundmass (Fig. 5*c*), and occurs in association with calcite, amphibole and allanite and pseudomorphed leucite. Hydro-zircon is present in all the dykes and is also present in the cores of pseudomorphed leucite as aggregates of very fine grains. Strontianite and dolomite are very rarely present as a groundmass phase in the VL4 and VL5 dykes.

Chlorite and quartz are present as a mesostasis material in almost all the dykes. Chlorite replaces groundmass phlogopite, amphibole and pyroxene. Relatively coarse-grained aggregates of quartz are commonly seen in the pseudomorphed phases after leucite. Cryptocrystalline $SiO_2$ is present in all dykes as a late-stage, anhedral groundmass phase.

Magnetite and pyrite (Fig. 7*b*) are observed in almost all the dykes in accessory amounts. Rarely present are very small anhedral crystals of Co-Ni-bearing chalcopyrite.

## Mineral compositions

### *Phlogopite*

Representative compositions of phlogopite are given in Table 2 and Supplementary Table 1. The cores of phenocrysts of phlogopites contain 10.8–10.5 wt.% $Al_2O_3$ and 4.8–4.7 wt.% $FeO_T$ with the rims being relatively depleted in $Al_2O_3$ (6.5–6.3 wt.%) and enriched in $FeO_T$ (15.0–13.5 wt.%). No significant difference exists between the $TiO_2$ contents of the core and rim of zoned phenocrysts and microphenocrysts (Table 2). The groundmass phlogopites and tetraferriphlogopites contain



https://doi.org/10.1180/minmag.2017.081.045 Published online by Cambridge University Press

TABLE 2. Representative compositions (wt.%) of phlogopites.

| Wt.% | 1<br>VL4 | 2<br>VL4 | 3<br>VL5 C | 4<br>VL5 R | 5<br>VL5 C | 6<br>VL5 R | 7<br>VL5 | 8<br>VL5 | 9<br>VL6 | 10<br>VL6 | 11<br>VL7 | 12<br>VL7 | 13<br>VL8 |
|---|---|---|---|---|---|---|---|---|---|---|---|---|---|
| $SiO_2$ | 40.99 | 40.68 | 41.65 | 41.66 | 41.53 | 41.20 | 41.96 | 40.07 | 39.55 | 39.74 | 39.68 | 39.08 | 42.29 |
| $TiO_2$ | 6.11 | 5.69 | 5.50 | 5.42 | 5.57 | 5.64 | 5.92 | 5.15 | 5.12 | 5.12 | 5.22 | 4.43 | 6.00 |
| $Al_2O_3$ | 6.43 | 7.31 | 10.77 | 6.33 | 10.53 | 6.45 | 6.01 | 8.03 | 8.57 | 7.13 | 7.40 | 8.40 | 5.25 |
| FeO(t) | 15.78 | 16.72 | 4.73 | 13.45 | 4.85 | 15.01 | 16.58 | 15.88 | 16.62 | 20.65 | 20.88 | 20.52 | 16.69 |
| MgO | 14.30 | 14.21 | 23.73 | 17.05 | 23.48 | 15.84 | 15.37 | 15.34 | 15.60 | 13.44 | 13.71 | 14.31 | 14.93 |
| $K_2O$ | 9.26 | 9.13 | 10.19 | 9.72 | 10.31 | 9.81 | 9.73 | 9.04 | 9.51 | 8.91 | 9.15 | 9.05 | 9.12 |
| BaO | 1.35 | 1.62 | 1.01 | 1.06 | 0.81 | 1.08 | 0.96 | 1.16 | 1.62 | 1.51 | n.d. | 1.22 | 1.54 |
| F | 1.72 | 1.23 | 1.60 | 1.82 | 1.68 | 1.46 | 1.12 | 0.99 | 0.67 | 0.76 | 1.02 | 0.92 | 1.09 |
| Total | 94.22 | 95.36 | 97.58 | 94.69 | 97.08 | 95.03 | 96.53 | 94.67 | 96.59 | 96.50 | 96.04 | 97.01 | 95.82 |
| Structural formula calculated on the basis of 16 cations | | | | | | | | | | | | | |
| Si | 6.557 | 6.443 | 5.992 | 6.492 | 6.005 | 6.453 | 6.514 | 6.314 | 6.119 | 6.279 | 6.230 | 6.081 | 6.670 |
| Ti | 0.735 | 0.678 | 0.595 | 0.635 | 0.606 | 0.664 | 0.691 | 0.610 | 0.596 | 0.608 | 0.616 | 0.518 | 0.712 |
| Al | 1.212 | 1.364 | 1.826 | 1.163 | 1.794 | 1.191 | 1.100 | 1.491 | 1.563 | 1.328 | 1.369 | 1.540 | 0.976 |
| Fe | 2.111 | 2.215 | 0.569 | 1.753 | 0.586 | 1.966 | 2.153 | 2.093 | 2.150 | 2.729 | 2.742 | 2.670 | 2.201 |
| Mg | 3.410 | 3.355 | 5.090 | 3.961 | 5.061 | 3.699 | 3.557 | 3.603 | 3.598 | 3.166 | 3.209 | 3.319 | 3.510 |
| K | 1.890 | 1.845 | 1.870 | 1.932 | 1.902 | 1.960 | 1.927 | 1.817 | 1.877 | 1.796 | 1.833 | 1.796 | 1.835 |
| Ba | 0.085 | 0.101 | 0.057 | 0.065 | 0.046 | 0.066 | 0.058 | 0.072 | 0.098 | 0.093 | – | 0.074 | 0.095 |
| F | 0.870 | 0.616 | 0.728 | 0.897 | 0.768 | 0.723 | 0.550 | 0.493 | 0.328 | 0.380 | 0.507 | 0.453 | 0.544 |

n.d. – not detected; FeO(t) –total Fe expressed as FeO; C – Core and R – Rim.

TABLE 3. Representative compositions (wt.%) of amphiboles.

| Wt.% | 1 VL2 | 2 VL2 C | 3 VL2 R | 4 VL3 | 5 VL6 | 6 VL6 | 7 VL7 | 8 VL7 | 9 VL8 C | 10 VL8 R1 | 11 VL8 R2 |
|---|---|---|---|---|---|---|---|---|---|---|---|
| $SiO_2$ | 52.46 | 52.74 | 53.75 | 54.00 | 53.02 | 50.61 | 48.97 | 51.03 | 52.36 | 52.27 | 53.83 |
| $TiO_2$ | 1.67 | 2.06 | 1.50 | 4.81 | 2.63 | 6.30 | 3.73 | 1.77 | 4.01 | 2.52 | 4.13 |
| $Al_2O_3$ | n.d. | n.d. | n.d. | 0.26 | 0.32 | 0.48 | 0.25 | 0.23 | n.d. | n.d. | n.d. |
| MnO | 0.38 | 0.29 | n.d. | n.d. | 0.32 | 0.19 | 0.52 | 0.45 | n.d. | n.d. | n.d. |
| FeO(t) | 22.66 | 16.49 | 18.40 | 19.11 | 16.20 | 13.75 | 22.19 | 25.30 | 8.71 | 14.71 | 14.51 |
| FeO | 20.01 | 15.53 | 18.40 | n.d. | 16.20 | 13.75 | 22.19 | 24.39 | 8.71 | 14.71 | 14.51 |
| $Fe_2O_3$ | 2.946 | 1.063 | n.d. | n.d. | n.d. | n.d. | n.d. | 1.01 | n.d. | n.d. | n.d. |
| MgO | 9.02 | 12.65 | 10.69 | 10.21 | 11.29 | 12.48 | 7.63 | 6.01 | 16.61 | 12.22 | 12.50 |
| CaO | 2.60 | 4.09 | 4.95 | 0.61 | 5.43 | 5.58 | 5.13 | 2.77 | 5.15 | 4.38 | 1.14 |
| $Na_2O$ | 5.29 | 4.62 | 6.67 | 7.12 | 4.14 | 3.94 | 4.29 | 5.16 | 3.89 | 4.44 | 6.92 |
| $K_2O$ | 5.05 | 5.07 | 4.97 | 0.45 | 5.08 | 5.09 | 4.89 | 4.91 | 5.34 | 5.16 | 5.08 |
| F | 0.64 | n.d. | n.d. | n.d. | 1.00 | 0.66 | n.d. | n.d. | 1.18 | 0.86 | n.d. |
| Structural formula calculated on the basis of 23 cations | | | | | | | | | | | |
| Formula assignments | K-AF | K-RT | K-RT | Ti-Mg- Rieb | K-KAT | Ti-K-KAT | K-Fe-RT | K-AF | K-RT | K-RT | Ti-K-Mg AF |
| T site Si | 7.917 | 7.878 | 7.924 | 7.876 | 7.904 | 7.517 | 7.655 | 7.978 | 7.745 | 7.954 | 7.946 |
| Al | – | – | – | 0.045 | 0.056 | 0.084 | 0.046 | 0.022 | – | – | – |
| Ti | 0.083 | 0.122 | 0.076 | 0.079 | 0.040 | 0.399 | 0.299 | | 0.255 | 0.046 | 0.054 |
| C site $Fe^{3+}$ | – | – | – | 0.000 | – | – | – | – | – | – | – |
| Ti | 0.107 | 0.110 | 0.090 | 0.449 | 0.255 | 0.305 | 0.139 | 0.208 | 0.191 | 0.243 | 0.405 |
| Al | – | – | – | – | – | – | – | 0.020 | – | – | – |
| $Fe^{3+}$ | 0.335 | 0.119 | – | 0.859 | – | – | – | 0.121 | – | – | – |
| $Mn^{2+}$ | 0.004 | 0.013 | – | – | 0.040 | 0.024 | 0.069 | 0.060 | – | – | – |
| $Fe^{2+}$ | 2.525 | 1.941 | 2.268 | 1.472 | 2.020 | 1.708 | 2.901 | 3.187 | 1.077 | 1.872 | 1.791 |
| Mg | 2.029 | 2.817 | 2.349 | 2.220 | 2.509 | 2.763 | 1.778 | 1.401 | 3.663 | 2.772 | 2.751 |
| $Mn^{2+}$ | 0.045 | 0.024 | – | – | – | – | – | – | – | – | – |
| B site Ca | 0.420 | 0.655 | 0.782 | 0.095 | 0.867 | 0.888 | 0.859 | 0.464 | 0.816 | 0.714 | 0.180 |
| Na | 1.535 | 1.322 | 1.218 | 1.905 | 1.133 | 1.112 | 1.141 | 1.536 | 1.116 | 1.286 | 1.820 |
| Ca | | | | | | | | | | | |
| A site Na | 0.013 | 0.016 | 0.688 | 0.109 | 0.064 | 0.023 | 0.159 | 0.028 | – | 0.024 | 0.161 |
| K | 0.972 | 0.966 | 0.935 | 0.084 | 0.966 | 0.964 | 0.975 | 0.979 | 1.008 | 1.002 | 0.957 |
| F | 0.305 | – | – | – | 0.471 | 0.310 | – | – | 0.552 | 0.414 | – |

n.d. – not detected; $Fe_2O_3$ and FeO calculated on a stoichiometric basis; C – Core; R – Rim.
K-AF: potassic-arfvedsonite; K-RT: potassic-richterite; Ti-Mg-Rieb: Ti rich Mg riebeckite; K-KAT: potassic-katophorite; Ti-K-KAT: Ti-rich potassic-katophorite; K-Fe-RT: potassic-ferro-richterite; Ti-K-Mg AF: Ti-rich potassic-magnesio-arfvedsonite.

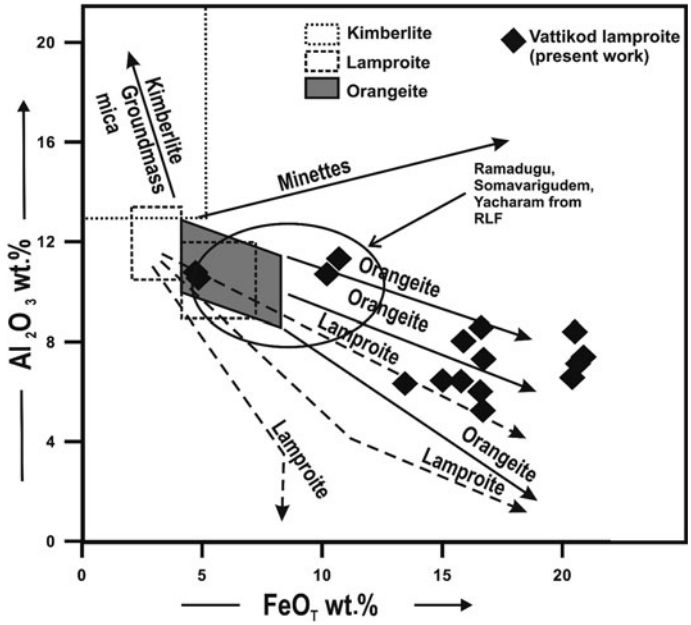


FIG. 8. $Al_2O_3$ *vs*. $FeO_T$ compositional variation of phlogopite in Vattikod lamproites. Also shown is the field for phlogopites from other Ramadugu lamproites. Compositional fields and trends for kimberlites, lamproite, orangeite and minette micas from Mitchell (1995).

8.6–5.3 wt.% $Al_2O_3$ and 20.9–15.8 wt.% $FeO_T$ and are enriched in $TiO_2$ (6.1–4.4 wt.%). The $Al_2O_3$ contents of Vattikod phlogopites compare well with the range of 5–11 wt.% $Al_2O_3$ reported for other lamproite phlogopites (Jaques *et al*., 1986; Mitchell, 1989; Mitchell and Bergman, 1991). The BaO contents of all micas are typically <2 wt.% and fluorine contents vary between 0.7–1.8 wt.% (Table 2).

The zoned phlogopite phenocrysts in VL5 are typical of lamproitic micas and the compositional zoning (core to rim) is a trend of decreasing $Al_2O_3$ and MgO with increasing $FeO_T$ (Table 2; Fig. 8). The tetraferriphlogopite rims are extremely enriched in $FeO_T$ and depleted in $Al_2O_3$ (Table 2). Following Mitchell and Bergman (1991) the compositional evolution is considered to be from octahedral site-deficient Ti-rich phlogopite to tetraferriphlogopite. Mica compositional zonation trends are similar to those found in orangeites (also known as Kaapvaal lamproite; Mitchell, 2006) and lamproites (Mitchell and Bergman, 1991; Figs 8, 9). The Vattikod phlogopites are more evolved than those in other Ramadugu lamproites (Figs 8, 9; Chalapathi Rao *et al*., 2014).

### *Amphibole*

The amphiboles exhibit a wide range in composition (Table 3 and Supplementary Table 2) and all have low $Al_2O_3$ (<0.5 wt.%) contents typical of most lamproite amphiboles (Mitchell and Bergman, 1991). They contain (6.3 to 1.5 wt.%) $TiO_2$, (7.1 to 3.9 wt.%) $Na_2O$, (5.3 to 0.5 wt.%) $K_2O$ and (25.3 to 8.7 wt.%) $FeO_T$ with fluorine contents up to 1.1 wt.%.

The amphiboles show compositional evolution from Ti-rich potassic-magnesio-katophorite through Ti-rich potassic-katophorite, potassic-katophorite, potassic-ferro-richterite and potassic-richterite to potassic-arfvedsonite (Table 3). Figures 10 and 11 show that the Vattikod amphiboles evolve to compositions that are far richer in $FeO_T$ than are typical of lamproites *sensu lato*, and are similar to evolved amphiboles from the Rice Hill lamproite (Mitchell and Bergman, 1991). The Vattikod amphiboles are also comparatively more evolved than those occurring in other Ramadugu lamproites (Figs 10, 11; Chalapathi Rao *et al*., 2014). Vattikod amphiboles are not compositionally equivalent to amphiboles in minettes, and other potassic rocks (Figs 10, 11; Mitchell and Bergman, 1991). The



https://doi.org/10.1180/minmag.2017.081.045 Published online by Cambridge University Press

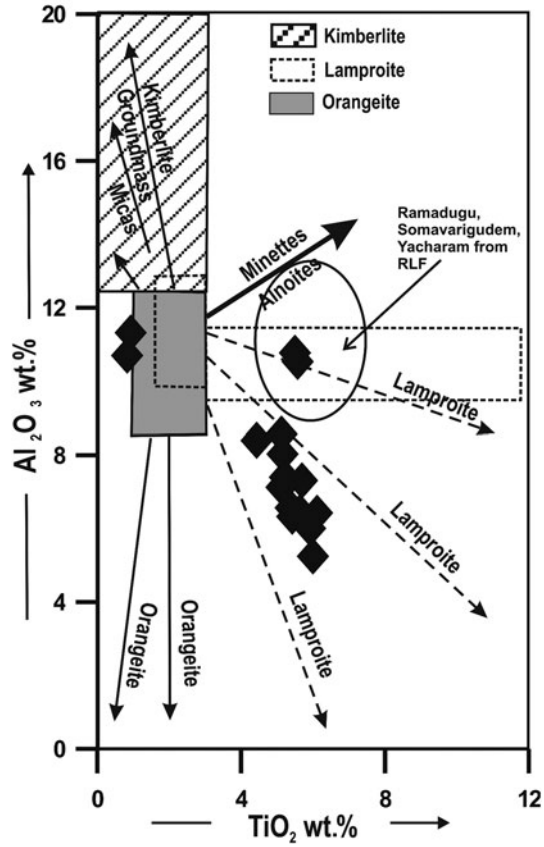


FIG. 9. $Al_2O_3$ *vs*. $TiO_2$ (wt.%) compositional variation of phlogopite in Vattikod lamproites. Also shown is the field for phlogopites from other Ramadugu lamproites. Compositional fields and trends for kimberlites, lamproite, orangeite and minette micas from Mitchell (1995).

extremely low $Al_2O_3$ content of the amphiboles is attributed to the low alumina contents of their parental peralkaline magma (Wagner and Velde, 1986; Mitchell and Bergman, 1991).

### *Clinopyroxene*

Representative compositions of clinopyroxenes are given in Table 4. Two compositionally distinct clinopyroxenes are present; diopside and Na-Fe-rich pyroxene. Diopsides commonly occur as phenocrysts and a groundmass phase as reported in many lamproites (Table 4; Jacques *et al*., 1986; Mitchell and Bergman, 1991). The sodic variety has been reported previously from Raniganj lamproites rimming diopside (Mitchell and Fareeduddin, 2009), although such iron-rich pyroxenes with (17.8–17.5 wt.%) $FeO_T$ and (1.3–0.4 wt.%) $Na_2O$ have not been reported from other lamproites (Table 3; Mitchell and Bergman, 1991). The Ti *vs*. Al diagram for all the varieties of clinopyroxenes clearly indicates their lamproitic affinity (Fig. 12).

### *K-feldspar*

Representative compositions of K-feldspar, Ba-K-feldspar (hyalophane) and Na-feldspar are given in (Table 5). The pseudomorphic K-feldspars are comparable in composition to K-feldspars in other lamproites (Mitchell and Bergman, 1991), and are relatively poor in $Na_2O$ (n.d.–0.3 wt.%) and $FeO_T$ (0.4–2.1 wt.%; Table 5). Ba-K-feldspar and Na-feldspar occur in the ovoid aggregates (Table 5). Ba-K feldspars (hyalophane) have been reported from the Raniganj lamproites (Mitchell and



https://doi.org/10.1180/minmag.2017.081.045 Published online by Cambridge University Press

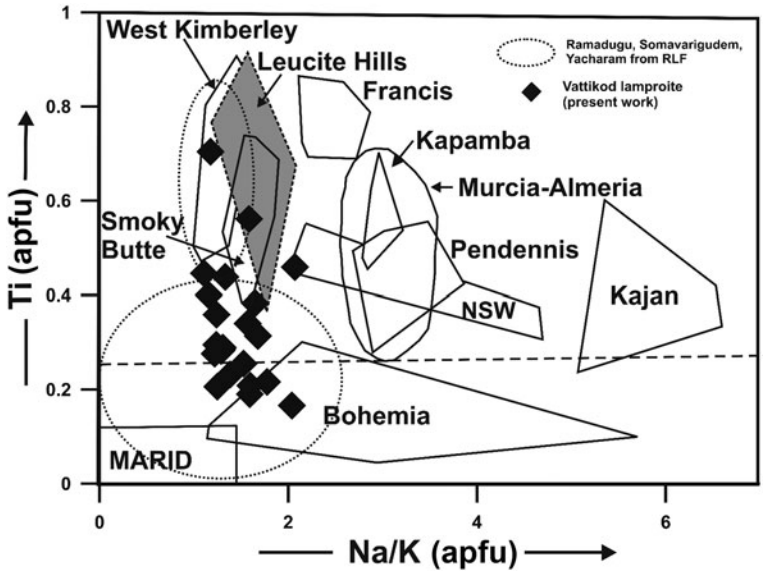


FIG. 10. Ti *vs*. Na/K (atoms per formula unit) compositional variation of amphiboles in Vattikode lamproites. The field for amphiboles from other Ramadugu lamproites is also shown. Compositional fields and trends for amphiboles in lamproites and other potassic rocks from Mitchell and Bergman (1991).

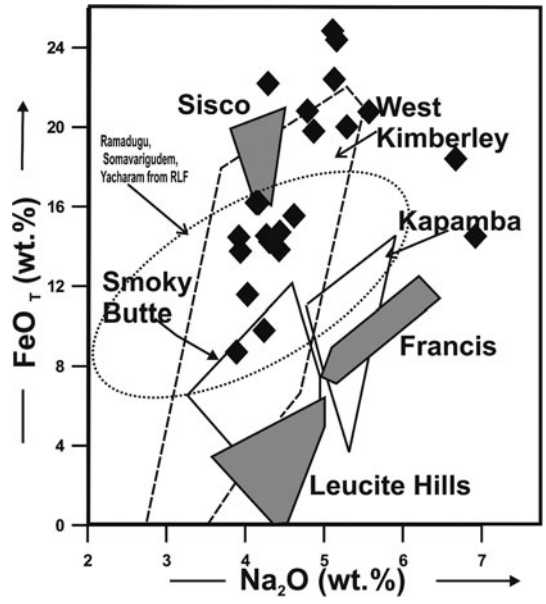


FIG. 11. $FeO_T$ *vs*. $Na_2O$ compositional variation of amphiboles from P-1 Vattikod lamproites. Also shown is the field for phlogopites from other Ramadugu lamproites. Compositional fields and trends for amphiboles in lamproites from Mitchell and Bergman (1991).



https://doi.org/10.1180/minmag.2017.081.045 Published online by Cambridge University Press

TABLE 4. Representative compositions (wt. %) of pyroxenes.

| Wt.% | 1<br>VL2 | 2<br>VL3 | 3<br>VL3 | 4<br>VL3 | 5<br>VL3 | 6<br>VL3 | 7<br>VL3 | 8<br>VL3 | 9<br>VL7 | 10<br>VL7 |
|---|---|---|---|---|---|---|---|---|---|---|
| $SiO_2$ | 55.48 | 54.36 | 54.29 | 54.23 | 54.18 | 54.57 | 54.46 | 55.55 | 54.61 | 53.78 |
| $TiO_2$ | 0.44 | 1.23 | 1.18 | 1.31 | 1.04 | 1.16 | 0.49 | 0.53 | 2.39 | 2.00 |
| $Al_2O_3$ | 0.65 | n.d. | n.d. | n.d. | n.d. | n.d. | 0.53 | 0.56 | 0.49 | 0.45 |
| FeO(t) | 9.19 | 3.21 | 2.89 | 2.85 | 3.72 | 3.09 | 17.52 | 17.80 | 4.17 | 4.08 |
| MgO | 20.39 | 17.02 | 17.10 | 17.25 | 17.16 | 17.44 | 13.32 | 14.25 | 16.25 | 16.37 |
| CaO | 12.88 | 24.23 | 24.15 | 24.06 | 24.40 | 24.19 | 10.79 | 11.21 | 22.09 | 23.27 |
| $Na_2O$ | n.d. | n.d. | n.d. | n.d. | n.d. | n.d. | 1.31 | 0.42 | n.d. | n.d. |
| Cr2O3 | n.d. | 0.57 | 0.57 | 0.66 | n.d. | 0.47 | n.d. | n.d. | 0.44 | 0.83 |
| Total | 99.03 | 100.62 | 100.18 | 100.36 | 100.50 | 100.92 | 98.42 | 100.32 | 100.44 | 100.78 |
| Structural formula calculated on the basis of 4 cations | | | | | | | | | | |
| Si | 2.046 | 1.981 | 1.985 | 1.979 | 1.974 | 1.979 | 2.093 | 2.105 | 2.009 | 1.970 |
| Ti | 0.012 | 0.034 | 0.032 | 0.036 | 0.028 | 0.032 | 0.014 | 0.015 | 0.066 | 0.055 |
| Al | 0.028 | – | – | – | – | – | 0.024 | 0.025 | 0.021 | 0.019 |
| Fe | 0.283 | 0.098 | 0.088 | 0.087 | 0.113 | 0.094 | 0.563 | 0.564 | 0.128 | 0.125 |
| Mg | 1.121 | 0.925 | 0.932 | 0.938 | 0.932 | 0.943 | 0.763 | 0.805 | 0.891 | 0.894 |
| Ca | 0.509 | 0.946 | 0.946 | 0.941 | 0.952 | 0.940 | 0.444 | 0.455 | 0.871 | 0.913 |
| Na | – | – | – | – | – | – | 0.098 | 0.031 | – | – |
| $Cr_2O_3$ | – | 0.016 | 0.016 | 0.019 | – | 0.013 | – | – | 0.013 | 0.024 |

n.d. – not detected; FeO(t) – total Fe expressed as FeO.

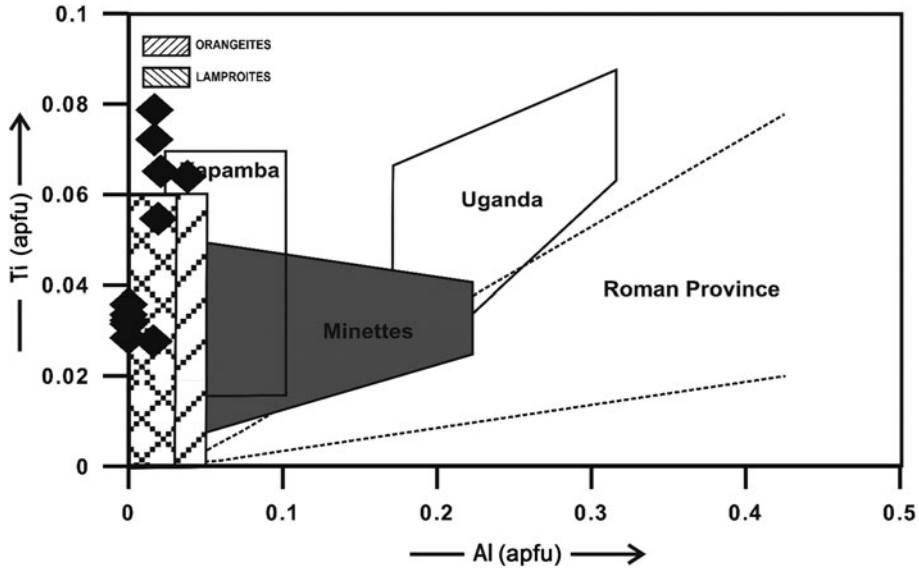


FIG. 12. Compositional variation (Ti *vs*. Al in atoms per formula unit) of pyroxenes from Vattikod lamproites. Compositional fields and trends for lamproites, minettes, Roman province lavas and kamafugites from Mitchell and Bergman (1991).

Fareeduddin, 2009). Na-feldspar has not been reported in earlier studies of lamproites.

### *Spinels*

Representative compositions of spinel are given in (Table 6). The spinels contain $Cr_2O_3$ (up to 53.0 wt.%), MgO (up to 4.2 wt.%), $FeO_T$ (up to 41.7 wt.%), $TiO_2$ (up to 6.6 wt.%) and ZnO (0.42 to 5.6 wt.%). All spinels are chromium-rich and represent principally solid solutions between chromite and magnetite with minor amounts of qandilite, ulvöspinel and franklinite. Most of the groundmass spinels are not zoned. Minor continuous core-to-rim zoning is one of decreasing MgO and $Cr_2O_3$ and increasing total FeO and ZnO at nearly constant to higher Ti (Table 6). The Vattikod spinel compositions are shown in Fig. 13, projected onto the front face of the reduced spinel prism (Mitchell, 1986). The extreme Ti-enrichment which is common for lamproite spinels is not observed for Vattikod spinels (Mitchell, 1995; Mitchell and Fareeduddin, 2009). Figure 13 shows that these spinels are unlike all kimberlite spinels but are similar to relatively unevolved Ti-poor spinels in lamproites and orangeites (lamproite var. Kaapvaal). Similar trends of spinel compositions have been reported for Raniganj lamproites (Mitchell and Fareeduddin, 2009) and also in ultramafic lamprophyres from Torngat (Tappe *et al*., 2004). In comparison to spinels found in other Ramadugu lamproites, the Vattikod spinels are more evolved in terms of Fe and Ti (Fig. 13; Chalapathi Rao *et al*., 2014). As most of the spinels are poor in alumina (<3.1 wt.%) and enriched in ZnO they indicate the peralkaline nature of the magma from which they crystallized, and their affinity to the lamproite clan.

### *Apatite and monazite*

Representative compositions of apatite are given in Table 7. The apatites are rich in SrO (up to 3.7 wt.%), and contain significant fluorine (up to 4.1 wt.%). They can be classified as fluorapatites, and are similar to those reported in many lamproites (Thy *et al*., 1987; Edgar, 1989; Mitchell and Bergman, 1991). They contain no barium and are poor in light-rare-earth elements. The sheaf-like quench apatites which are scattered throughout the groundmass of Vattikod lamproites are too small for quantitative analysis.

Representative compositions of monazite-(Ce) are given in Table 7. The monazite is enriched in $Ce_2O_3$ (up to 34 wt.%), SrO (<2 wt.%) and with (up to 2 wt.%) $ThO_2$. Monazites of similar composition have also been reported from the Raniganj lamproites (Mitchell and Fareeduddin, 2009).



https://doi.org/10.1180/minmag.2017.081.045 Published online by Cambridge University Press

TABLE 5. Representative compositions (wt.%) of K-feldspar, Na-feldspar and Ba-K-feldspar.

| Wt.% | 1<br>VL1 | 2<br>VL2 | 3<br>VL3 | 4<br>VL4 | 5<br>VL5 | 6<br>VL6 | 7<br>VL7 | 8<br>VL8 | 9<br>VL3 | 10<br>VL4 |
|---|---|---|---|---|---|---|---|---|---|---|
| $SiO_2$ | 65.16 | 64.36 | 65.62 | 64.86 | 65.84 | 65.22 | 64.82 | 65.47 | 67.07 | 54.59 |
| $Al_2O_3$ | 18.57 | 17.82 | 18.01 | 17.25 | 17.77 | 18.07 | 17.25 | 17.64 | 18.99 | 19.76 |
| FeO(t) | 0.39 | 1.35 | 0.61 | 2.10 | 0.44 | 0.82 | 1.58 | 0.46 | 0.24 | n.d. |
| $Na_2O$ | n.d. | 0.29 | n.d. | 0.20 | n.d. | n.d. | 0.18 | n.d. | 13.15 | 0.35 |
| $K_2O$ | 16.08 | 15.67 | 16.08 | 15.11 | 15.91 | 15.54 | 16.10 | 16.04 | n.d. | 12.66 |
| BaO | n.d. | n.d. | n.d. | n.d. | n.d. | n.d. | n.d. | n.d. | n.d. | 11.31 |
| Total | 100.20 | 99.49 | 100.32 | 99.52 | 99.96 | 99.65 | 99.93 | 99.61 | 99.45 | 98.67 |
| Structural formula calculated on the basis of 8 atoms of oxygens | | | | | | | | | | |
| Si | 3.000 | 3.000 | 3.020 | 3.020 | 3.034 | 3.016 | 3.017 | 3.032 | 2.970 | 2.782 |
| Al | 1.008 | 0.979 | 0.977 | 0.947 | 0.965 | 0.985 | 0.946 | 0.963 | 0.991 | 1.187 |
| Fe | 0.015 | 0.053 | 0.023 | 0.082 | 0.017 | 0.032 | 0.061 | 0.018 | 0.009 | – |
| Na | – | – | – | 0.018 | – | – | 0.016 | – | 1.129 | 0.035 |
| K | 0.945 | 0.932 | 0.944 | 0.898 | 0.935 | 0.917 | 0.956 | 0.948 | 0.000 | 0.823 |
| Ba | – | – | – | – | – | – | – | – | – | 0.226 |

n.d. – not detected; FeO(t) – total Fe expressed as FeO.

TABLE 6. Representative compositions (wt.%) of spinels.

| Wt.% | 1<br>VL1 | 2<br>VL2 | 3<br>VL3 | 4<br>VL4 | 5<br>VL5 | 7<br>VL6 | 9<br>VL7 | 10<br>VL10 | 11<br>VL7 C | 12<br>VL7 R | 13<br>VL8 C | 14<br>VL8 R |
|---|---|---|---|---|---|---|---|---|---|---|---|---|
| $TiO_2$ | 5.55 | 4.09 | 4.31 | 3.98 | 4.68 | 5.14 | 5.55 | 6.64 | 4.94 | 5.61 | 3.70 | 5.29 |
| $Al_2O_3$ | 2.00 | 2.88 | 1.94 | 1.88 | 2.19 | 2.08 | 2.07 | 1.40 | 1.97 | 2.01 | 3.07 | 2.16 |
| FeO(t) | 38.81 | 34.56 | 37.56 | 35.97 | 39.47 | 39.79 | 38.70 | 41.74 | 37.93 | 38.71 | 32.40 | 35.56 |
| FeO | 30.61 | 29.05 | 27.96 | 28.99 | 32.37 | 33.53 | 32.60 | 34.62 | 31.68 | 31.75 | 26.40 | 28.42 |
| $Fe_2O_3$ | 9.11 | 6.12 | 10.67 | 7.76 | 7.89 | 6.96 | 6.78 | 7.92 | 6.94 | 7.73 | 6.67 | 7.93 |
| MnO | 2.07 | 2.02 | 1.83 | 1.90 | 2.10 | 2.14 | 2.29 | 1.69 | 1.93 | 2.05 | 1.97 | 2.29 |
| MgO | 2.77 | 0.61 | 0.30 | n.d. | 0.51 | 0.95 | 0.62 | 2.60 | 2.76 | 2.57 | 4.15 | 1.02 |
| ZnO | 0.60 | 3.83 | 5.56 | 5.33 | 3.63 | 2.24 | 4.60 | 0.42 | 1.41 | 2.02 | 1.23 | 4.83 |
| $Cr_2O_3$ | 47.98 | 49.57 | 45.15 | 50.03 | 45.98 | 45.35 | 45.81 | 44.06 | 48.57 | 46.96 | 53.02 | 47.01 |
| Total | 100.69 | 98.17 | 97.72 | 99.87 | 99.35 | 98.39 | 100.32 | 99.34 | 100.21 | 100.70 | 100.21 | 98.95 |
| Structural formula calculated on the basis of 32 atoms of oxygens | | | | | | | | | | | | |
| Ti | 1.203 | 0.923 | 0.988 | 0.894 | 1.047 | 1.155 | 1.230 | 1.461 | 1.075 | 1.218 | 0.793 | 1.187 |
| Al | 0.680 | 1.018 | 0.697 | 0.661 | 0.768 | 0.732 | 0.719 | 0.483 | 0.672 | 0.684 | 1.032 | 0.759 |
| $Fe2^+$ | 7.380 | 7.288 | 7.128 | 7.238 | 8.054 | 8.377 | 8.033 | 8.473 | 7.666 | 7.665 | 6.295 | 7.091 |
| $Fe3^+$ | 1.978 | 1.381 | 2.446 | 1.742 | 1.765 | 1.564 | 1.502 | 1.743 | 1.512 | 1.679 | 1.430 | 1.780 |
| Mn | 0.505 | 0.513 | 0.472 | 0.480 | 0.529 | 0.542 | 0.571 | 0.419 | 0.473 | 0.501 | 0.476 | 0.579 |
| Mg | 1.190 | 0.273 | 0.136 | – | 0.226 | 0.423 | 0.272 | 1.134 | 1.190 | 1.106 | 1.764 | 0.454 |
| Zn | 0.128 | 0.848 | 1.251 | 1.175 | 0.797 | 0.494 | 1.001 | 0.091 | 0.301 | 0.430 | 0.259 | 1.064 |
| Cr | 10.936 | 11.756 | 10.881 | 11.809 | 10.814 | 10.712 | 10.671 | 10.195 | 11.111 | 10.717 | 11.951 | 11.087 |

n.d. – not detected; FeO(t) – total Fe expressed as FeO; C – core and R – Rim.

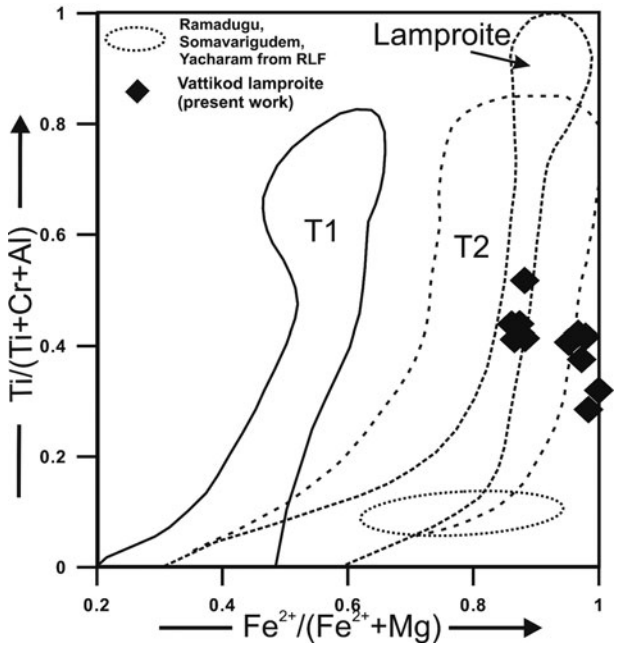


FIG. 13. Compositional variation of spinels from Vattikod lamproites projected onto the front face of the reduced iron spinel compositional prism (Mitchell, 1986). Compositional fields and trends for spinels from kimberlites (T1) and lamproites (T2) from Mitchell (1986, 1995).

Monazites have not been reported from Vattikod lamproite dykes by earlier workers (Kumar *et al*., 2013*a*) or from other Ramadugu lamproites (Chalapathi Rao *et al*., 2014).

## Discussion and conclusions

We consider that bulk-rock geochemistry of these mineralogically complex and altered rocks cannot be used to characterize their parental magmas. The best way to characterize them is by consideration of their typomorphical mineralogy (Mitchell, 1991; Mitchell and Tappe, 2010) as given in Table 8.

The Vattikod mineral assemblage and their compositions are comparable to those of lamproites *sensu lato* in terms of the presence of pseudoleucite, phlogopite–tetraferriphlogopite, K-Na-Ti amphibole, Al-poor clinopyroxene, apatite and spinels. The Vattikod lamproites do not contain fresh olivine but pseudomorphs after olivine are considered to be present on the basis of their morphology. Priderite and other Ti and K zirconium minerals (Mitchell and Bergman, 1991) have not been recognized in the Vattikod dykes. The dykes have also undergone diverse degrees of deuteric alteration which is evident by the development of secondary phases such as titanite, allanite, hydro-zircon, calcite, chlorite, quartz and cryptocrystalline $SiO_2$. The formation of titanite and allanite along the cleavages and margins of pseudomorphed phases is rarely observed in VL4 and VL5 dykes which also have very minor anhedral secondary titanite in comparison to other Vattikod dykes, thus indicating these to be the least altered dykes. In addition VL4 and VL5 dykes preserve fresh phlogopite and alteration to chlorite is very limited in comparison to other Vattikod dykes. All of the 'leucite' which was present as phenocrysts and groundmass phase, is now completely pseudomorphed by K-feldspar and secondary phases.

Taking into account the textural and mineralogical account of the various dykes we conclude that VL4 and VL5 are the least altered followed with increasing degrees of alteration by VL6, VL7, VL8, VL2, VL3, VL10 and V1. We classify the Vattikod dykes VL4 and VL5 as pseudoleucite-phlogopite-lamproite; VL2 and VL3 as pseudoleucite-amphibole-lamproite; VL6, VL7 and VL8 as pseudoleucite-phlogopite-amphibole-lamproite.



https://doi.org/10.1180/minmag.2017.081.045 Published online by Cambridge University Press

TABLE 7. Representative compositions (wt.%) of apatites and monazites.

| Wt.% | 1<br>VL 1 | 2<br>VL2 | 3<br>VL3 | 4<br>VL4 | 5<br>VL5 | 6<br>VL6 | 7<br>VL7 | 8<br>VL8 | 9<br>VL10 | 10<br>VL4 | 11<br>VL4 | 12<br>VL5 | 13<br>VL5 |
|---|---|---|---|---|---|---|---|---|---|---|---|---|---|
| $P_2O_5$ | 40.48 | 40.05 | 41.02 | 40.59 | 41.28 | 40.81 | 40.10 | 39.72 | 40.82 | 30.31 | 30.65 | 30.42 | 31.10 |
| $SiO_2$ | 0.64 | 0.67 | 1.02 | 1.99 | 0.93 | 1.43 | 1.22 | 2.19 | 1.16 | 1.12 | 1.82 | 2.02 | 2.38 |
| FeO(t) | 0.24 | 0.30 | n.d. | n.d. | n.d. | n.d. | 0.32 | n.d. | n.d. | n.d. | n.d. | 0.73 | 0.42 |
| CaO | 51.23 | 51.25 | 52.79 | 52.11 | 52.63 | 52.95 | 50.23 | 50.74 | 51.38 | n.d. | n.d. | n.d. | n.d. |
| SrO | 2.65 | 3.30 | 2.59 | 2.46 | 2.95 | 2.29 | 3.30 | 3.66 | 2.80 | 1.23 | 1.12 | 1.31 | 1.77 |
| $La_2O_3$ | n.d. | n.d. | n.d. | 0.49 | n.d. | 0.44 | 0.60 | n.d. | 0.47 | 18.31 | 17.09 | 21.01 | 19.56 |
| $Ce_2O_3$ | n.d. | n.d. | 0.56 | 1.12 | 0.68 | 0.93 | 1.19 | 0.94 | 0.83 | 34.16 | 33.34 | 32.85 | 32.87 |
| $Nd_2O_3$ | n.d. | n.d. | n.d. | 0.36 | 0.39 | 0.37 | 0.47 | 0.57 | 0.48 | 8.26 | 8.78 | 6.63 | 8.00 |
| $Pr_2O_3$ | n.d. | n.d. | n.d. | n.d. | n.d. | n.d. | n.d. | n.d. | n.d. | 3.13 | 3.09 | 2.72 | 2.95 |
| $ThO_2$ | n.d. | n.d. | n.d. | n.d. | n.d. | n.d. | n.d. | n.d. | n.d. | 0.86 | 1.70 | 0.65 | 0.25 |
| F | 4.05 | 3.93 | 2.89 | 3.20 | 3.36 | 3.61 | 3.30 | 3.26 | 3.18 | n.d. | n.d. | n.d. | n.d. |
| Total | 95.24 | 95.57 | 97.98 | 99.12 | 98.86 | 99.22 | 97.43 | 97.82 | 97.94 | 97.38 | 97.59 | 98.34 | 99.30 |

1–9: apatites; 10–13 monazites; n.d. – not detected; FeO(t) – total Fe expressed as FeO.

As VL1 is completely altered the precursor mineralogy cannot be identified. VL10 is also extensively altered but contains fresh euhedral apatite microphenocrysts together with pseudomorphs after leucite and is classified as a pseudoleucite-apatite-(phlogopite?) lamproite.

The amphiboles, phlogopites and spinels of the Vattikod dykes are more evolved in comparison to those in the Ramadugu, Yacharam and Somavarigudem lamproites of the Ramadugu lamproite field (Figs 8, 9, 10, 11 and 13; Chalapathi Rao *et al*., 2014). The presence of monazite and allanite indicates enrichment in rare-earth elements of the batch of magma from which these dykes rocks evolved.

Although these rocks have many of the mineralogical characteristics of lamproites (*sensu lato*), they are subtly different in terms of local mineralogical variation. Thus, the amphibole compositions are atypical of amphiboles from many lamproites in terms of their low $TiO_2$ and high $FeO_T$ contents, although they are similar to Raniganj and Ramadugu amphiboles (Mitchell and Bergman, 1991; Mitchell and Fareeduddin, 2009; Chalapathi Rao *et al*., 2014). The overall compositional trend of spinels in these rocks is also similar to that found in lamproites, although it differs in that the Vattikod spinels have relatively low Ti/(Ti + Cr + Al) ratios of <0.6 and are enriched in Zn.

Notable differences between lamproites (*sensu lato*) and the Vattikod rocks include the presence of rutile, titanite, allanite, monazite, hydro-zircon, quartz and cryptocrystalline $SiO_2$ as a late-stage groundmass and alteration minerals. However, the textural and mineralogical data demonstrates that in terms of a mineralogical-genetic classification the Vattikod dykes are *bona fide* lamproites. It is suggested that the Vattikod lamproites represent a spectrum of modal variants of lamproite produced by the differentiation and crystallization of a common parental peralkaline potassic magma. The magma from which the dykes were formed is best regarded as the expression of a particular variety of cratonic potassic magmatism derived from a local metasomatized mantle source (Mitchell, 2006). Similar conclusions have been drawn for the Wajrakurur P2-West, P5, P12, P13, TK1 and TK4 intrusions in the Eastern Dharwar craton which are now reclassified as lamproite, and for the Raniganj dykes of the Gondwana coal fields (Mitchell, 2006; Mitchell and Fareeduddin, 2009; Gurmeet Kaur and Mitchell, 2013; Gurmeet Kaur *et al*., 2013; Gurmeet Kaur and Mitchell, 2016; Shaikh *et al*., 2016). Further study of the Ramadugu



https://doi.org/10.1180/minmag.2017.081.045 Published online by Cambridge University Press

TABLE 8. List of minerals present in Vattikod lamproite dykes.

| | Minerals | VL1 | VL2 | VL3 | VL4 | VL5 | VL6 | VL7 | VL8 | VL10 |
|---|---|---|---|---|---|---|---|---|---|---|
| 1 | Phlogopite | | | | √ | √ | √ | √ | √ | |
| 2 | Amphibole | | √ | √ | | | √ | √ | √ | |
| 3 | Pyroxene | | √ | √ | | | | √ | | |
| 4 | K-feldspar | √ | √ | √ | √ | √ | √ | √ | √ | √ |
| 5 | Spinel | √ | √ | √ | √ | √ | √ | √ | √ | √ |
| 6 | Titanite | √ | √ | √ | √ | √ | √ | √ | √ | √ |
| 7 | Apatite | √ | √ | √ | √ | √ | √ | √ | √ | √ |
| 8 | Monazite | | | | √ | √ | | | | |
| 9 | Allanite | √ | √ | √ | √ | √ | √ | √ | √ | √ |
| 10 | Rutile | √ | √ | √ | √ | √ | √ | √ | √ | |
| 11 | Calcite | √ | √ | √ | √ | √ | √ | √ | √ | √ |
| 12 | Baryte | √ | √ | √ | √ | √ | √ | √ | √ | √ |
| 13 | Hydro-zircon | √ | √ | √ | √ | √ | √ | √ | √ | √ |
| 14 | Chlorite | √ | √ | √ | √ | | √ | √ | √ | √ |
| 15 | $SiO_2$ | √ | √ | √ | √ | √ | √ | √ | √ | √ |
| 16 | Dolomite | | | | √ | √ | | | | |
| 17 | Magnetite | | √ | √ | √ | √ | √ | √ | √ | |
| 18 | Pyrite | | √ | √ | √ | √ | √ | √ | | |
| 19 | Co-Ni-sulfide | | √ | √ | | | | | | |

√ – present.

lamproite field as a whole, and in conjunction with the Krishna and Cuddapah Basin lamproites and also other peralkaline rocks occurring in the Eastern Dharwar Craton and adjoining Eastern Ghats Mobile Belt is required to establish in greater detail the inter-field mineralogical variation and the evolution of the parental peralkaline magmas in this south-eastern segment of southern India.

We have previously proposed a link between the disposition of 'Deformed Alkaline Rocks and Carbonatites' commonly known as DARC's (Burke and Khan, 2006) of the Eastern Ghats Mobile Belt and the lamproites of the Eastern Dharwar Craton (Fig. 1; Leelanandam *et al*., 2006; Burke and Khan, 2006; Gurmeet Kaur and Mitchell, 2016). The near-linear disposition of DARC's and lamproites has been interpreted to imply a relationship with ancient subduction-related processes (Fig 1; Das Sharma and Ramesh, 2013; Gurmeet Kaur and Mitchell, 2016). Das Sharma and Ramesh (2013) have reported the presence of relict subducted oceanic slab material at depths of 160–220 km in the subcontinental lithospheric mantle. This subducted oceanic slab is considered to be a product of suturing of the Eastern Dharwar Craton and Eastern Ghats Mobile Belt at ~1600 Ma. This timing is appropriate for the later emplacement of all lamproites in the Eastern Dharwar Craton between 1100–1450 Ma (Gopalan and Kumar, 2008; Osborne *et al*., 2011; Chalapathi Rao *et al*., 2013; Chalapathi Rao *et al*., 2014). Although we have no geochronological data we see no reason why the Vattiokod dykes should not belong to this general period of lamproite magmatism. Clearly, any ancient subducted material, if metasomatized in Proterozoic times, could provide a source for the lamproitic magmatism. Recently, Dongre *et al*. (2015) have proposed a subduction-related origin for Archaean eclogite xenoliths from the Wajrakarur kimberlite field in the Eastern Dharwar Craton. We note that the extensive near-linear disposition of the east Indian lamproites is not in accord with the ascent of a mantle plume as a mechanism for causing partial melting of potential sources. In conclusion we propose that the Vattikod and other lamproites in eastern India emplaced at 1100–1450 Ma are possible manifestations of ancient subduction-related alkaline magmatism along the Eastern Ghats Mobile Belt as also has been proposed for 1.2 Ga Krishna lamproites (Fig. 1) in the neighbourhood of Ramadugu lamproites by Chakrabarti *et al.* (2007) on the basis of Nd–Hf–Pb isotopic characteristics, low $SiO_2$, high Mg-numbers, low $Al_2O_3/TiO_2$, high $CaO/Al_2O_3$, high $TiO_2$, high Ni, Cr, Th/U and Nb/Th–Nb/U ratios. This proposition is in contrast to extension-related anorogenic lamproite magmatism related to supercontinent(s) break-up, as has been suggested for Ramadugu and other Dharwar Craton lamproites (Chalapathi Rao *et al*., 2014). We do not consider that these rocks are Mediterranean-type lamproites or that they were formed in active subduction zones. We merely speculate that the material involved in the formation of their source regions was ancient subducted material in common with other lamproitic magmas (Mitchell and Bergman, 1991).

## Acknowledgements

This work was supported by the Natural Sciences and Engineering Research Council of Canada, Almaz Petrology, and Lakehead University, Ontario, Canada. Gurmeet Kaur acknowledges Panjab University, Chandigarh, India for granting leave to pursue research on Indian lamproites at Lakehead University. We gratefully acknowledge Prof. S. Tappe, Dr. Teresa Ubide and Prof. Adrian Finch for their suggestions in improving this manuscript.

## Supplementary material

To view supplementary material for this article, please visit https://doi.org/10.1180/minmag.2017.081.045

## References

Ahmed, S. and Kumar, A. (2012) *Search for kimberlite/lamproite in Paluvayi block in Nalgonda district, Andhra Pradesh*. Geological Survey of India Report, Kolkata, India.

Burke, K. and Khan, S. (2006) Geoinformatic approach to global nepheline syenite and carbonatite distribution: testing a Wilson cycle model. *Geosphere*, **2**, 53–60.

Chalapathi Rao, N.V. and Srivastava, R.K. (2016) Kimberlites, lamproites, lamprophyres, carbonatites, other alkaline rocks and mafic dykes from the Indian Shield: Glimpses of research (2012–2016). *Proceedings Indian National Science Academy*, **82** (3), 515–536.

Chalapathi Rao, N.V., Gibson, S.A., Pyle, D.M., Dickin, A.P. (2004) Petrogenesis of Proterozoic lamproites and kimberlites from the Cuddapah Basin and Dharwar craton, southern India. *Journal of Petrology*, **45**(5), 907–948.

Chakrabarti, R., Basu, A.R. and Paul, D.K. (2007) Nd-Hf-Sr-Pb isotopes and trace element geochemistry of Proterozoic lamproites from southern India: subducted

komatiite in the source. *Chemical Geology*, **236**, 291–302.

Chalapathi Rao, N.V., Creaser, R.A., Lehmann, B. and Panwar, B.K. (2013) Re-Os isotope study of Indian kimberlites and lamproites: Implications for mantle source and cratonic evolution. *Chemical Geology*, **353**, 36–47.

Chalapathi Rao, N.V., Kumar, A., Sahoo, S., Dongre, A. N. and Talukdar, D. (2014) Petrology and petrogenesis of Mesoproterozoic lamproites from the Ramadugu field, NW margin of the Cuddapah basin, Eastern Dharwar craton, southern India. *Lithos*, **196–197**, 150–168.

Conticelli, S. (1998) The effect of crustal contamination on ultrapotassic magmas with lamproitic affinity: mineralogical, geochemical and isotope data from the Torre Alfina lavas and xenoliths, central Italy. *Chemical Geology*, **149**, 51–81.

Das Sharma, S. and Ramesh, D.S. (2013) Imaging mantle lithosphere for diamond prospecting in southeast India. *Lithosphere*, **5**, 331–342.

Davies, G.R., Stolz, A.J., Mahotkin, I.L., Nowell, G.M. and Pearson, D.G. (2006) Trace element and Sr–Pb–Nd–Hf isotope evidence for ancient, fluid-dominated enrichment of the source of Aladan shield lamproites. *Journal of Petrology*, **47**, 1119–1146.

Dongre, A.N., Jacob, D.E. and Stern, R.A. (2015) Subduction-related origin of eclogite xenoliths from the Wajrakarur kimberlite field, Eastern Dharwar craton, Southern India: Constraints from petrology and geochemistry. *Geochimica et Cosmochimica Acta*, **166**, 165–188.

Edgar, A.D. (1989) Barium- and strontium-enriched apatites in lamproites from West Kimberley, Western Australia. *American Mineralogist*, **74**, 889–895.

Fareeduddin and Mitchell, R.H. (2012) *Diamonds and their Source Rocks in India*. Geological Society of India, Bangalore, India. 434 pp.

Fritschle, T., Prelević, D., Foley, S.F. and Jacob, D.E. (2013) Petrological characterization of the mantle source of Mediterranean lamproites: Indications from major and trace elements of phlogopite. *Chemical Geology*, **353**, 267–279.

Gopalan, K. and Kumar, A. (2008) Phlogopite K–Ca dating of Narayanpet kimberlites, South India: implications to the discordance between their Rb–Sr, Ar/Ar ages. *Precambrian Research*, **167**, 377–382.

Gupta, S., Rai, S.S., Prakasam, K.S., Srinagesh, D., Chadha, R.K., Priestley, K. and Gaur, V.K. (2003) First evidence for anomalous thick crust beneath mid-Archaean western Dharwar craton. *Current Science*, **84**, 1219–1226.

Gurmeet Kaur and Mitchell, R.H. (2013) Mineralogy of the P2-West "Kimberlite", Wajrakarur kimberlite field, Andhra Pradesh, India: kimberlite or lamproite? *Mineralogical Magazine*, **77**, 3175–3196.

Gurmeet Kaur and Mitchell, R.H. (2016) Mineralogy of the P-12 K-Ti-richterite diopside olivine lamproite from Wajrakarur, Andhra Pradesh, India: implications for subduction-related magmatism in eastern India, *Mineralogy and Petrology*, **110**, 223–245.

Gurmeet Kaur, Korakoppa, M., Fareeduddin and Pruseth, K.L. (2013) Petrology of P-5 and P-13 "kimberlites" from Lattavaram kimberlite cluster, Wajrakarur Kimberlite Field, Andhra Pradesh, India: Reclassification as lamproites. Pp 183–194 in: *Proceedings of the X$^{th}$ International Kimberlite Conference* (D.G. Pearson, H.S. Grutter, J.W. Harris, B.A. Kjarsgaard, H. O'brien, N.V Chalapathi Rao and R.S.J. Sparks). Geological Society of India, Springer Publication.

Gurmeet Kaur, Mitchell, R.H. and Ahmed, S. (2016) Typomorphic mineralogy of the Vattikod lamproites from Mesoproterozoic Ramadugu Lamproite Field, Nalgonda District, Telangana, India: A plausible manifestation of subduction-related alkaline magmatism in the Eastern Ghats Mobile Belt? *35$^{th}$ International Geological Congress*, Abstract #3482. Available at: https://www.americangeosciences.org/igc/15421

Jaques, A.L., Lewis, J.D. and Smith, C.B. (1986) *The Kimberlites and Lamproites of Western Australia*. Geological Survey of Western Australia Bulletin, **132**.

Kumar, A., Ahmed, S., Priya, R. and Sridhar, M. (2013*a*) Discovery of lamproites near Vattikod area, NW margin of the Cuddapah basin, Eastern Dharwar craton, southern India. *Journal of the Geological Society of India*, **82**, 307–312.

Kumar, B. Niraj, Zeyen, H., Singh, A.P. and Singh, B. (2013*b*) Lithospheric structure of southern Indian shield and adjoining oceans: integrated modelling of topography, gravity, geoid and heat flow data. *Geophysical Journal International*, **194**, 30–44.

Leelanandam, C., Burke, K., Ashwal, L.D. and Webb, S.J. (2006) Proterozoic mountain building in Peninsular India: an analysis based primarily on alkaline rock distribution. *Geological Magazine*, **143**, 195–212.

Liferovich, R.P. and Mitchell, R.H. (2005) Composition and paragenesis of Na-, Nb-, and Zr-bearing titanite from Khibina, Russia, and crystal structure data for synthetic analogues. *Canadian Mineralogist*, **43**, 795–812.

Mirnejad, H. and Bell, K. (2006) Origin and source evolution of the Leucite Hills lamproites: evidence from Sr–Nd–Pb–O isotopic compositions. *Journal of Petrology*, **47**, 2463–2489.

Mitchell, R.H. (1986) *Kimberlites: Mineralogy, Geochemistry and Petrology.* Plenum Press, New York and London, 442 pp.

Mitchell, R.H. (1989) Compositional variation of micas from the Leucite hills lamproites. *28$^{th}$ International Geological Congress*. Washington, USA. Extended Abstract **2**, pp. 446–447.



https://doi.org/10.1180/minmag.2017.081.045 Published online by Cambridge University Press

Mitchell, R.H. (1991) *Kimberlites and Lamproites: Primary Source of Diamond*. Geoscience Canada Reprint series **6**, pp. 8–28.

Mitchell, R.H. (1995) *Kimberlites, Orangeites, and Related Rocks*. Plenum press. New York, 410 pp.

Mitchell, R.H. (2006) Potassic magmas derived from metasomatized lithospheric mantle: Nomenclature and relevance to exploration for diamond-bearing rocks. *Journal Geological Society of India*, **67**, 317–327.

Mitchell, R.H. and Bergman, S.C. (1991) *Petrology of Lamproites*. Plenum Press, New York, 447pp.

Mitchell, R.H. and Fareeduddin (2009) Mineralogy of peralkaline lamproites from the Raniganj Coalfield, India. *Mineralogical Magazine*, **73**, 457–477.

Mitchell, R.H. and Tappe, S. (2010) Discussions of 'Kimberlites and aillikites as probes of the continental lithospheric mantle'. *Lithos*, **109**, 72–80.

Murphy, D.T., Collerson, K.D. and Kamber, B.S. (2002) Lamproites from Gaussberg, Antarctica: Possible transition zone melts of Archaean subducted sediments. *Journal of Petrology*, **43**, 981–1001.

Neelkantam, S. (2001) Exploration for diamonds in southern India. *Geological Survey of India Special Publication*, **58**, 521–555.

Nowell, G.M., Pearson, D.G., Bell, D.R., Carlson, R.W., Smith, C.B., Kempton, P.D. and Noble, S.R. (2004) Hf isotope systematics of kimberlites and their megacrysts: New constraints on their source regions. *Journal of Petrology*, **45**, 1583–1612.

Osborne, I., Sherlock, S., Anand, M. and Argles, T. (2011) New Ar–Ar ages of southern Indian kimberlites and a lamproite and their geochemical evolution. *Precambrian Research*, **189**, 91–103.

Perez-Valera, L.A., Rosenbaum, G., Sanchez-Gomez, M., Azor, A., Fernandez-Soler, J.M., Perez-Valera, F. and Vasconcelos, P.M. (2013) Age distribution of lamproites along the Socovos Fault (southern Spain) and lithospheric scale tearing. *Lithos*, **180–181**, 252–263.

Prelevic, D., Foley, S.F., Romer, R.L. and Conticelli, S. (2008) Mediterranean Tertiary lamproites derived from multiple source components in postcollisional geodynamics. *Geochimica et Cosmochimica Acta*, **72**, 2125–2156.

Rapp, R.P., Irifune, T., Shimizu, N., Nishiyama, N., Norman, M.D. and Inoue, J. (2008) Subduction recycling of continental sediments and the origin of geochemically enriched reservoirs in the deep mantle. *Earth Planetary Science Letters*, **271**, 14–23.

Roy, S. and Mareschal, J.C. (2011) Constraints on the deep thermal structure of the Dharwar craton, India, from heat flow, shear wave velocities, and mantle xenoliths. *Journal of Geophysical Research*, **116**, 1–15.

Shaikh, A.M., Patel, S.C., Ravi, S., Behera, D. and Pruseth, K.L. (2016) Mineralogy of the TK1and TK4 'kimberlite' in the Timmasamudram cluster, Wajrakarur Kimberlite Field, India: Implications for lamproite magmatism in a field of kimberlites and ultramafic lamprophyres. *Chemical Geology*, **455**, 208–230.

Sridhar, M. and Rau, T.K. (2005) Discovery of a new lamproite field Ramadugu lamproite field (RLF), Nalgonda District, Andhra Pradesh. *Proceedings of the Group Discussion on Kimberlites and Related Rocks of India*. Organized by the Geological Society of India, Bangalore, pp. 55–57 (Extended abstracts).

Tainton, K.M. and Mckenzie, D. (1994) The generation of kimberlites, lamproites and their source rocks. *Journal of Petrology*, **35**, 787–817.

Tappe, S., Jenner, G.A., Foley, S.F., Heaman, L., Besserer, D., Kjarsgaard, B.A. and Ryan, B. (2004) Torngat ultramafic lamprophyres and their relation to the North Atlantic Alkaline Province. *Lithos*, **76**, 491–518.

Tappe, S, Foley, S.F., Jenner, G.A., Heaman, L.M., Kjarsgaard, B.A., Romer, R.L., Stracke, A., Joyce, N. and Hoefs, J. (2006) Genesis of ultramafic lamprophyres and carbonatites at Aillik Bay, Labrador: a consequence of incipient lithospheric thinning beneath the North Altantic craton. *Journal of Petrology*, **47**, 1261–1315.

Tappe, S., Foley, S.F., Stracke, A., Romer, R.L., Kjarsgaard, B.A., Heaman, L.M. and Joyce, N. (2007) Craton reactivation on the Labrador sea margins: 40Ar/39Ar age and Sr-Nd-Hf-Pb isotope constraints from alkaline and carbonatites intrusive. *Earth and Planetary Science Letters*, **256**, 433–454.

Tappe, S., Pearson, D.G. and Prevelic, D. (2013) Kimberlite, carbonatite, and potassic magmatism as part of the geochemical cycle. *Chemical Geology*, **353**, 1–3.

Tappe, S., Kjarsgaard, B.A., Kurszlaukis, S., Nowell, G. and Phillips, D. (2014) Petrology and Nd-Hf isotope geochemistry of the Neoproterozoic Amon kimberlite sills, Baffin Island (Canada): Evidence for deep mantle magmatic activity linked to supercontinent cycles. *Journal of Petrology*, **55**, 2003–2042.

Thy, P., Stecher, O. and Korstgard, J.A. (1987) Mineral chemistry and crystallization sequences in kimberlite and lamproite dikes from the Sisimut area, central west Greenland. *Lithos*, **20**, 391–417.

Tommasini, S., Avanzinelli, R. and Conticelli, S. (2011) The Th/La and Sm/La conundrum of the Tethyan realm lamproites. *Earth and Planetary Science Letters*, **301**, 469–478.

Wagner, C. and Velde, D. (1986) The mineralogy of K-richterite-bearing lamproites. *American Mineralogist*, **71**, 17–37.

Zurevinski, S.E. and Mitchell, R.H. (2011) Highly evolved hypabyssal kimberlite sills from Wemindji, Quebec, Canada: insights into the process of flow differentiation in kimberlite magmas. *Contributions to Mineralogy and Petrology*, **161**, 765–776.



https://doi.org/10.1180/minmag.2017.081.045 Published online by Cambridge University Press